

# University of Reading

School of Mathematics, Meteorology & Physics

## FINITE ELEMENT MODELLING OF THE ATMOSPHERE USING THE SHALLOW WATER EQUATIONS

Alastair J. Radcliffe

August 2007

---

A dissertation submitted in partial fulfilment of the requirements for the degree of  
Master of Science.

## **Abstract**

A continuous-discontinuous barotropic finite element based model is developed for the simulation of synoptic scale atmospheric dynamics using the shallow water equations in spherical coordinates. Linear conforming and non-conforming basis functions are introduced to represent a continuous elevation and a discontinuous velocity field respectively, allowing improved performance through the avoidance of spurious computational modes and a Discontinuous Galerkin formulation of momentum advection. Time integration is based on a fully explicit 3rd order Adams Bashforth scheme. The resulting model does not require any matrix inversion due to the lumping of the elevation mass matrix and the orthogonality of the non-conforming basis functions. Results are shown for standard test cases specified in Williamson et al.(1992).

A.J.Radcliffe (May 2007)

## **Declaration**

I confirm that this work is my own and the use of all other material from other sources has been properly and fully acknowledged.

Signed

.....

Alastair J. Radcliffe

Dated

.....

## Contents

<b>Abstract</b>	<b>2</b>
<b>Declaration</b>	<b>3</b>
<b>Introduction</b>	<b>8</b>
Atmospheric Model Requirements . . . . .	8
Rotating Frames of Reference . . . . .	9
The Material Derivative . . . . .	9
The Shallow Water Equations . . . . .	10
Discretization methods . . . . .	11
Flow Derivative Constructions . . . . .	12
Eulerian Schemes . . . . .	13
Full Lagrangian Schemes . . . . .	13
Semi-Lagrangian Schemes . . . . .	13
Summary . . . . .	14
<b>Formulations</b>	<b>15</b>
The Governing Equations . . . . .	15
Scaling . . . . .	15
Spherical Coordinates . . . . .	17
Weak Formulations . . . . .	20
Continuous Elevation Form . . . . .	20
Continuous Velocity Form . . . . .	20
Boundary Terms . . . . .	20
Eulerian Non-linear Simplification . . . . .	21
Finite Element Spatial Discretization . . . . .	22
Linear Conforming Basis Functions . . . . .	22
Linear Non-Conforming Basis Functions . . . . .	23
Summations . . . . .	24
Testing the Continuous Elevation Weak Formulation . . . . .	24
Momentum Equation . . . . .	24
Mass Equation . . . . .	26
Time Discretization . . . . .	27
Upwinding . . . . .	27
Artificial Diffusion . . . . .	29
<b>Numerical Experiments</b>	<b>32</b>
Introduction . . . . .	32
Test Case One: Pure Advection of a Cosine Bell . . . . .	32
Test Case Five: Zonal Flow over an Isolated Mountain . . . . .	35
Test Case Six: Rossby Haurwitz Wave . . . . .	35

<i>USING THE SHALLOW WATER EQUATIONS</i>	5
Test Case Seven: 500 mbar Geopotential Height and Wind Field Initial Conditions . . . . .	36
<b>Conclusions</b>	<b>46</b>
Future Work . . . . .	46

## Index of Symbols

$x$	.....	CARTESIAN ABCISSA
$y$	.....	CARTESIAN ORDINATE
$z$	.....	CARTESIAN VERTICAL COORDINATE
$r$	.....	SPHERICAL RADIAL COORDINATE
$\lambda$	.....	SPHERICAL AZIMUTH -LONGITUDE
$\theta$	.....	SPHERICAL DECLINATION -LATITUDE
$\mathbf{i}$ or $\mathbf{e}_x$	.....	CARTESIAN ABCISSA UNIT VECTOR
$\mathbf{j}$ or $\mathbf{e}_y$	.....	CARTESIAN ORDINATE UNIT VECTOR
$\mathbf{k}$ or $\mathbf{e}_z$	.....	CARTESIAN VERTICAL UNIT VECTOR
$\mathbf{e}_r$	.....	SPHERICAL RADIAL UNIT VECTOR
$\mathbf{e}_\lambda$	.....	SPHERICAL AZIMUTH UNIT VECTOR
$\mathbf{e}_\theta$	.....	SPHERICAL DECLINATION UNIT VECTOR
$\mathbf{r}$	.....	GENERAL POSITION VECTOR
$t$	.....	TIME VARIABLE
$\mathbf{u}$	.....	(HORIZONTAL) FLUID VELOCITY VECTOR
$h$	.....	FLUID (ATMOSPHERIC) DEPTH
$\nu$	.....	VISCOSITY COEFFICIENT
$\rho$	.....	HOMOGENEOUS FLUID DENSITY
$h_0$	.....	TOPOGRAPHIC DEPTH/HEIGHT
$f$	.....	CORIOLIS PARAMETER
$g$	.....	GRAVITATIONAL ACCELERATION = $9.81 \text{ m s}^{-2}$
$\boldsymbol{\Omega}$	.....	EARTH'S ROTATION VECTOR
$a$	.....	SPHERICAL EARTH RADIUS = $6.3675 \times 10^6 \text{ m}$
$\Omega$	.....	ANGULAR ROTATION RATE = $7.2921 \times 10^{-5} \text{ s}^{-1}$
$H$	.....	FLUID DEPTH SCALE FACTOR
$H_0$	.....	TOPOGRAPHIC DEPTH SCALE FACTOR
$U$	.....	SURFACE FLUID VELOCITY SCALE FACTOR
$T$	.....	TIME SCALE FACTOR
$L$	.....	SURFACE LENGTH SCALE FACTOR
$F$	.....	CORIOLIS PARAMETER SCALE FACTOR
$\tilde{t}$	.....	DIMENSIONLESS TIME COORDINATE
$\tilde{\mathbf{u}}$	.....	DIMENSIONLESS FLUID VELOCITY
$\tilde{h}$	.....	DIMENSIONLESS FLUID DEPTH
$\tilde{h}_0$	.....	DIMENSIONLESS TOPOGRAPHIC HEIGHT
$\tilde{f}$	.....	DIMENSIONLESS CORIOLIS PARAMETER
$\tilde{\mathbf{r}}$	.....	DIMENSIONLESS GENERAL POSITION VECTOR
$Ro$	.....	ROSSBY NUMBER
$Ro_T$	.....	TEMPORAL ROSSBY NUMBER

$E_k$	.....	EKMAN NUMBER
$\Omega$	.....	COMPUTATIONAL DOMAIN
$\partial\Omega$	.....	BOUNDARY OF COMPUTATIONAL DOMAIN
$d\tau$	.....	INCREMENTAL VOLUME ELEMENT
$ds$	.....	INCREMENTAL SURFACE AREA ELEMENT
$\mathbf{n}$	.....	SURFACE NORMAL TO $\partial\Omega$
$\mathcal{L}^2(\Omega)$	.....	SET OF SQUARE INTEGRABLE FUNCTIONS OVER $\Omega$
$\mathcal{H}$	.....	THE SET $\{h \in \mathcal{L}^2(\Omega) : \int_{\Omega} h \, d\tau = 0\}$
$\mathcal{U}$	.....	THE SET $\{\mathbf{u} \in \mathcal{L}^2(\Omega) \times \mathcal{L}^2(\Omega) : \mathbf{u} \cdot \mathbf{n} = 0\}$
$\mathcal{U}^w$	.....	THE SET $\{\mathbf{u} \in \mathcal{L}^2(\Omega) \times \mathcal{L}^2(\Omega)\}$
$\xi$	.....	CANONICAL TRIANGLE ABCISSA
$\eta$	.....	CANONICAL TRIANGLE ORDINATE
$\phi_i$	.....	$P_1$ LINEAR CONFORMING SHAPE FUNCTION
$\psi_i$	.....	$P_1^{NC}$ LINEAR NON-CONFORMING SHAPE FUNCTION
$\tilde{\mathcal{L}}^2(\Omega)$	.....	PIECEWISE SQUARE INTEGRABLE FUNCTIONS OVER $\Omega$
$h^h$	.....	DISCRETE ELEVATION APPROXIMATION
$\mathbf{u}^h$	.....	DISCRETE VELOCITY APPROXIMATION
$\mathcal{H}^h$	.....	THE SET $\{h^h \in \tilde{\mathcal{L}}^2(\Omega) : \int_{\Omega} h^h \, d\tau = 0\}$
$\mathcal{U}^h$	.....	THE SET $\{\mathbf{u}^h \in \tilde{\mathcal{L}}^2(\Omega) \times \tilde{\mathcal{L}}^2(\Omega) : \mathbf{u}^h \cdot \mathbf{n} = 0\}$
$\mathcal{U}^{wh}$	.....	THE SET $\{\mathbf{u}^h \in \tilde{\mathcal{L}}^2(\Omega) \times \tilde{\mathcal{L}}^2(\Omega)\}$
$\hat{h}$	.....	GENERIC ELEVATION TESTING FUNCTION
$\hat{\mathbf{u}}$	.....	GENERIC VELOCITY TESTING FUNCTION

## Introduction

### Atmospheric Model Requirements

Given that the Earth's atmosphere is one of the most complicated dynamical systems in the universe, it is (at present) impossible to capture all its processes accurately, be they rheologic, thermodynamic and so forth, within the same computational framework. Thus it is usually necessary to consider great simplifications, whereby most of the dynamical processes of the atmosphere are ignored, and design a computational model that supports little more than the particular dynamical phenomena of interest.

Theoretically, the full dynamics of the atmosphere are governed by the viscous non-linear equations of Navier-Stokes and the laws of thermodynamics, however, the level of complexity that these equations capture is rarely found in atmospheric models, and the most complete set of equations commonly used, derived from the above and from which most other model equation sets are derived, are known as the 'primitive equations'. The 'primitive' referring to the equation's expression in terms of the directly measureable primitive variables -pressure, velocity, density and temperature. These have been discretized with finite differences [6], with finite elements [5], [7], [25], finite volumes [3] and using spectral methods [11]. Some early examples of the integration of these 'complete' equations using a spherical geometry may be found in [16].

For the current work, we are concerned with the large (synoptic) scale horizontal motions of the atmosphere that have a large influence on the development and motions of synoptic scale features such as high and low pressure systems, jets and cyclones. Some of the most interesting features in this regime are fast gravity waves and slow Rossby waves, and so our choice of model must allow for the existence of both, but without the undue complications of trying to additionally represent the vertical motions in the atmosphere, which otherwise occur on a very different velocity scale [23], [10].

It would furthermore be expedient to choose a model with a governing set of equations that are also incompressible, this would avoid any difficulties with the propagations of fast compressible waves and their consequent impact on the choice of time-step with which to perform the temporal integrations.

The last requirement that we will make of our model is that it allow the conservation of potential vorticity in a barotropic atmosphere free from the effects of friction. This is a fundamental mechanism through which much of the synoptic scale structure of the atmosphere may be described [23], and for this final requirement, the model equations will be required to be inviscid.

The Shallow Water Equations may be demonstrated to satisfy all the above requirements [23]. However, before introducing them, it is first necessary to introduce a few concepts relevant to their description and use on the rotating sphere that may be used to represent the Earth.

## Rotating Frames of Reference

To avoid undue complications, most atmospheric models employ a coordinate reference frame that is considered to rotate with the angular velocity representative of that of the Earth. To do otherwise would necessitate the construction of large and cumbersome expressions for quantities such as velocities, which would prove difficult to work with.

As will be indicated later, Newton's second law lies behind one of the governing equations, that relating to momentum, for the shallow water model, but is only intended to be applied in an inertial reference frame that exhibits no accelerations. The law may be applied in the non-inertial rotating reference frame, with inherent accelerations towards the centre, in the usual (inertial) manner provided two extra 'artificial' forces are included in the momentum equation derived from it.

The first of these artificial forces is usually referred to as a 'centripetal force'. It is considered to act in a direction opposite to that of gravity at every point on the Earth and is a conservative force, allowing it to be represented by a scalar gradient. Because of the centripetal forces relative weakness compared to the gravitational force, which is also conservative, it is often (and will be here to) included with it via a 'reduced' gravity potential [8].

The second artificial force is termed the 'Coriolis force' after the work of Gaspard Gustave Coriolis and is found to always act in a direction perpendicular to a given fluid element's motion [8]. As such, the force never does any work, as might be anticipated given its artificial nature, but its influence accounts for the swirly nature of large-scale atmospheric flows and is consequently very important in all studies of synoptic scale atmospheric dynamics.

## The Material Derivative

The second important concept that needs to be considered before the shallow water equations themselves may be introduced is that of the material derivative.

For many fluid flow applications it is extremely useful to consider the temporal changes of a given quantity connected with a given fluid element moving with the flow itself, rather than with respect to some point fixed relative to the particular coordinate system chosen. The derivative associated with such changes is referred to as a 'material' (or sometimes 'total' or 'Lagrangian') derivative, and it may be expressed in terms of the usual static ('Eulerian') derivative, associated with changes at a given position, by

$$\frac{D}{Dt} = \frac{\partial}{\partial t} + \mathbf{u} \cdot \nabla \quad (1.1)$$

where  $\mathbf{u}$  refers to the velocity of a hypothetical fluid element to which the differentiated variable is to be associated.

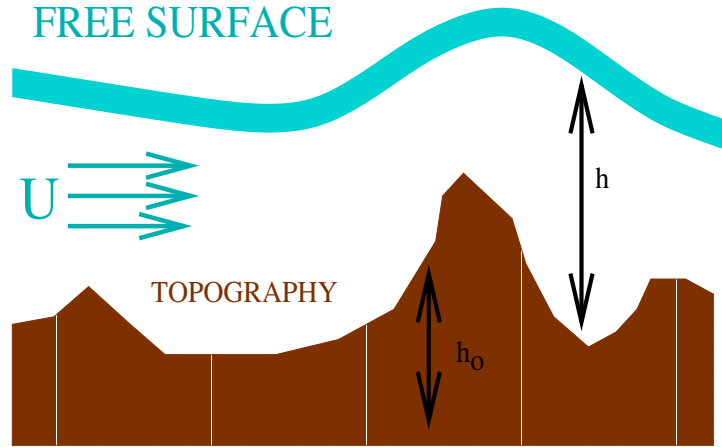


Figure 1: Shallow Water Parameters

## The Shallow Water Equations

With the material derivative and the fictitious forces found with rotating frames of reference established, we may now introduce the shallow water equations themselves with reference to the parameters depicted in Figure 1.

As indicated earlier, the equations themselves may be derived from the most general Navier-Stokes equation under the assumptions that the fluid flow of interest is both incompressible and inviscid, and through use of the hydrostatic approximation for a barotropic atmosphere [23]. This last assumption that level surfaces of pressure and density coincide thus removes any vertical fluid velocities associated with unstable density variations.

The viscous shallow water equations in a uniformly rotating reference frame may be summarized by the following conservation laws

- Conservation of mass

$$\frac{\partial h}{\partial t} + \nabla \cdot (h\mathbf{u}) = 0 \quad (1.2)$$

- Conservation of Momentum (Newton's second law)

$$\frac{\partial (h\mathbf{u})}{\partial t} + \nabla \cdot (h\mathbf{u}\mathbf{u}) = -\mathbf{\Omega} \times (h\mathbf{u}) - gh\nabla (h + h_0) + \frac{\nu}{h}\nabla \cdot (h\nabla\mathbf{u}) \quad (1.3)$$

where  $f$  is the Coriolis parameter and  $h$  refers to the height of a fluid column above a (topographic) surface level of  $h_0$  (defined with respect to some reference), moving with velocity  $\mathbf{u}$  subject to a reduced gravitational acceleration  $g$ . Note that for an incompressible fluid, conservation of mass is equivalent to the conservation of volume.

This viscous form of the shallow water equations has been introduced, even though we have required our governing equations to be inviscid, in order to show

the position the viscous diffusion term would otherwise occupy. Ideally, and in most of what follows, the viscosity *shall* be considered sufficiently small for the effects of diffusion to be neglected. However, it will be seen that for some problems, a small ‘artificial’ diffusion is needed to stabilize the solution.

For atmospheric modelling, a ‘geopotential height’ is often referred to. This simply refers to the multiplication of the fluid’s height (or depth),  $h$ , measured in meters, say, with the gravitational acceleration  $g$ , in meters per second squared. The units of geopotential height are thus meters squared per second squared, or  $[m][m/s^2] = [m^2/s^2]$ .

For the geopotentials we will be concerned with, the values of these heights are typically of the order  $10^6 m^2/s^2$ . This will be reflected in the scale analysis of the equations performed later and in the results sections, where this is often the factor used to scale the results.

## Discretization methods

For any numerical model, once the equations are established, consideration needs to be focussed on the exact method by which they will be discretized, in both time and space (temporally and spatially).

There are three primary approaches that have been used to discretize the shallow water equations on the global sphere relevant to the atmospheric modelling of interest here.

The first of these methods is by far the most popular in atmospheric simulations, and is known as the ‘Finite Difference Method’ (FDM). Details of its implementation may be found in [1] and [22].

For the purposes of global simulations on a closed sphere, however, this method suffers from a very poor node distribution around the north and south poles, though there have been early attempts to overcome this problem [16]. However, finite difference methods do have the advantage of only allowing interactions between neighbouring unknown values of the solution field, resulting in sparse system matrices.

Also employing only local interactions is the Finite Element Method [2]. This method has tended to be more popular in other scientific fields than in the atmospheric sciences. This last fact is perhaps a little surprising given that it has all the advantages of the Finite Difference Method, but without any of the node distribution problems.

It is thus the method adopted here, especially as, for future work, it may also accommodate deliberate non-uniform node positioning to capture accurately features in the solution that appear at different scales without undue computational effort, so called ‘mesh adaptivity’ [2].

A distinct advantage of the finite element method is also in the ease with which it is possible to create and manipulate high-order interpolations to the unknown

solution and to implement adaptive meshing techniques [17]. While such techniques have been applied recently with great success to atmospheric models [20], for the present work only linear (first-order) finite elements will be used.

Closely related to the finite element method is the ‘finite volume method’. It has the same node distribution advantages of the finite element method, but works entirely in terms of the local fluxes between ‘cells’ [3], [27], taking advantage of the conservation properties of governing conservative equations. However, for finite volumes, unlike for finite elements, there is no minimization principle through which the fluxes between elements can influence the formulation of the discrete equations. The similarities (and differences) in performances of these last two schemes with respect to solution advection has been examined for ocean modelling [14] where advection has an even greater dominance than in atmospheric dynamics.

The last discretization method that shall be mentioned here, for completeness, are ‘Spectral Element Methods’ [11], [26]. These techniques use expansions of the unknown solution fields in terms of high-order spherical harmonic functions and Legendre transforms to replace spatial variations with variations in a ‘spectral’ plane in a Fourier like manner.

In this transformed environment, derivative construction is trivial and very accurate, however, the nature of the transformation operators means that interactions between disparate locations on the sphere are possible. Such ‘global interactions’ result in dense system matrices that require ‘fast’ techniques for their inversion if computational costs are not to become prohibitive.

Furthermore, to accommodate any non-linear advection term found in the governing equations, it is usually necessary to transform to and from the transformed spectral world repeatedly within each single iteration, and this can add to the computational costs. Finally, due to the nature of the spectral operators, topographic representations can sometimes be prone to ‘Gibbs effects’, preventing the accurate representation of relatively small scale topographic features.

## Flow Derivative Constructions

Once a spatial discretization scheme has been decided on, for any system of equations that involves non-linear advection, there is then a choice between three different methods to accommodate such advection, each with their own particular advantages and disadvantages.

Two of these methods handle the advection ‘implicitly’, whereby the advective term appearing in (1.3) is not discretized directly, however, the first method described is that adopted for the present work, and does discretize the non-linear term directly.

### **Eulerian Schemes**

These schemes have the great advantage of allowing the same mesh to be used to calculate the solution throughout the time duration being solved for. Because there is no need to remesh the computational domain during the solution process, the mesh is often referred to as ‘static’.

Such a mesh also permits ‘static derivatives’, so the combinations of solution values at different points in the computational domain required to form the derivatives used in the computation of the solution need only be established at the beginning of the solution process.

For large scale flow problems, the stabilization of gravity waves can be the prime concern, but it should be noted that the explicit handling of the difficult non-linear term by Eulerian methods, however, can sometimes require small timesteps, relative to the next methods, and thus necessitates possibly relatively many iterations to compute comparable durations of solution. But, as shall be seen, each iteration is quite cheap to compute.

### **Full Lagrangian Schemes**

In a completely opposite manner, full-Lagrangian schemes allow the mesh nodes to be advected from their initial positions by the flow, necessitating a remeshing, and interpolation of the solution onto such a new mesh, at each and every iteration.

By following the flow, however, the method exploits the structure of the material derivative to allow the easy (but indirect) accomodation of the non-linear term appearing within it. This allows the use of relatively large time-steps.

But a big disadvantage of full Lagrangian methods, and the reason why they are not so popular in practice, is that for all but the most trivial flows, complicated fluid parcel trajectories can eventually lead to poorly resolved or discretized region of the computational domain, so-called ‘voids’, where few (if any) mesh nodes have been advected and where the solution is all but unknowable.

### **Semi-Lagrangian Schemes**

The final method for handling the non-linear advection term is often thought of as combining the best bits of the two previous schemes, and is known as the ‘Semi-Lagrangian Method’. It has been applied to finite element models of the shallow water equations by [4], [17] (the latter using adaptive methods), and finite volume schemes by [21].

Like the Eulerian scheme, it makes use of a ‘static’ mesh, but much larger timesteps are possible because, like the full Lagrangian scheme, the structure of the material derivative is used by considering the advection of fluid parcels to a given mesh point during a single timestep.

This necessitates tracing back the path (corresponding to the characteristic of the underlying equations) of the fluid element arriving at a given mesh node, to

determine its location one timestep earlier. The solution at that location, which is highly unlikely to coincide with a mesh node, is then deemed to have been advected to the current position.

The principle disadvantage of the method is in the interpolation required at the foot of the characteristics to determine the value of the solution to be advected. This interpolation needs to be high order to avoid excessive dissipation [18], and thus can be expensive to compute, with a loss of mass (and violation of mass conservation) unless the interpolation scheme has been specifically designed to be conservative.

## Summary

For the present work we shall be using the shallow water equations in spherical polar coordinates to capture all the large scale horizontal motions of the atmosphere that we are interested in.

Finite elements in an Eulerian context will be used to allow an even node distribution over the surface of the spherical representation of the Earth and to keep the effects of dissipation controlled while keeping interactions between the solution values at different points strictly local, with the consequent reductions in computational effort required per solution iteration.

Furthermore, anticipating steep solution gradients that can generate unphysical oscillations with the more traditional, continuous finite elements, a non-conforming finite element that permits a discontinuous velocity field is introduced.

This new type of element allows a higher degree of flexibility in the solution enabling a dissipation of high order oscillations and a consequent improvement in numerical stability [14].

Results will be generated from an existing Eulerian shallow water finite element code that has been adapted, principally through the introduction of spherical polar coordinates, to enable simulations of synoptic scale atmospheric dynamics.

## Formulations

We start the formulations by establishing the exact form of the shallow water equations that will be adopted for all subsequent analysis, what will be referred to throughout the following as the ‘governing equations’.

### The Governing Equations

A simple expansion of the momentum equation (1.3) with the (neglected) viscous diffusion term in square braces gives

$$\begin{aligned} h \frac{\partial \mathbf{u}}{\partial t} + \underbrace{\mathbf{u} \frac{\partial h}{\partial t} + \mathbf{u} \nabla \cdot (h \mathbf{u})}_{=0} + h \mathbf{u} \cdot \nabla \mathbf{u} \\ = -h \boldsymbol{\Omega} \times \mathbf{u} - gh \nabla h - gh \nabla h_0 + \left[ \frac{\nu}{h} \nabla \cdot (h \nabla \mathbf{u}) \right] \end{aligned} \quad (2.1)$$

the statement of mass conservation (1.2) may then be used to eliminate the second and third terms on the left hand side.

Dividing (2.1) through by  $h$  and introducing the Coriolis parameter  $f$  by

$$\boldsymbol{\Omega} = f \mathbf{k} \quad (2.2)$$

allows the momentum equation for the shallow water equations to be expressed in a non-conservative form using both material and static partial derivatives in a uniformly rotating reference frame

$$\frac{D \mathbf{u}}{Dt} + f \mathbf{k} \times \mathbf{u} = -g \nabla (h + h_0) + \left[ \frac{\nu}{h} \nabla \cdot (h \nabla \mathbf{u}) \right] \quad (2.3)$$

which, together with the statement of mass conservation (1.2)

$$\frac{\partial h}{\partial t} + \nabla \cdot (h \mathbf{u}) = 0 \quad (2.4)$$

capture all of the physical fluid phenomena that will be investigated in this report.

### Scaling

To facilitate the understanding of the mechanisms at work within the shallow water equations, it is common practice to identify some characteristic scales for all of the variables involved.

These scales may be thought of as taking the form of scalar factors which assume the dimensions of their associated variables, and allow the introduction of dimensionless variables whose values vary about unity.

For the problem at hand, we introduce seven such quantities as follows

$$\begin{aligned}
h &= H\tilde{h} \\
\mathbf{u} &= U\tilde{\mathbf{u}} \\
t &= T\tilde{t} \\
\mathbf{r} &= L\tilde{\mathbf{r}} \\
h_0 &= H_0\tilde{h}_0 \\
f &= F\tilde{f}
\end{aligned} \tag{3.1}$$

Substituting these relations into the momentum equation (2.3) with the material derivative expanded out according to (1.1)

$$\begin{aligned}
&\frac{U}{T} \frac{\partial \tilde{\mathbf{u}}}{\partial \tilde{t}} + \frac{U^2}{L} \tilde{\mathbf{u}} \cdot \nabla \tilde{\mathbf{u}} + FU\tilde{f}\mathbf{k} \times \tilde{\mathbf{u}} \\
&= -\frac{gH}{L} \nabla \tilde{h} - \frac{gH_0}{L} \nabla \tilde{h}_0 + \left[ \frac{\nu U}{L^2} \frac{1}{\tilde{h}} \tilde{\nabla} \cdot (\tilde{h} \tilde{\nabla} \tilde{\mathbf{u}}) \right]
\end{aligned} \tag{3.2}$$

Following convention, because the principle force in large scale atmospheric flow is that due to the Coriolis effect, we free the Coriolis term completely from dimensions by dividing through by  $FU$

$$\begin{aligned}
&\frac{1}{FT} \frac{\partial \tilde{\mathbf{u}}}{\partial \tilde{t}} + \frac{U}{FL} \tilde{\mathbf{u}} \cdot \nabla \tilde{\mathbf{u}} + \tilde{f}\mathbf{k} \times \tilde{\mathbf{u}} \\
&= -\frac{gH}{FUL} \nabla \tilde{h} - \frac{gH_0}{FUL} \nabla \tilde{h}_0 + \left[ \frac{\nu}{F} \frac{1}{L^2} \frac{1}{\tilde{h}} \tilde{\nabla} \cdot (\tilde{h} \tilde{\nabla} \tilde{\mathbf{u}}) \right]
\end{aligned} \tag{3.3}$$

allowing us to identify the Rossby number

$$Ro = \frac{U}{FL} \tag{3.4}$$

and its temporal counterpart

$$Ro_T = \frac{1}{FT} \tag{3.5}$$

and also the Ekman number relevant to viscous diffusion

$$E_k = \frac{\nu}{FL^2} \tag{3.6}$$

To simplify the right hand side, we may take the topographic scaling  $H_0$  to be similar to that of the atmosphere,  $H$ , and set

$$\frac{gH}{FUL} = 1 \tag{3.7}$$

with the height, length and Coriolis scales determined by the problem, this then sets the typical velocity scale to be

$$U = \frac{gH}{FL} \quad (3.8)$$

Finally, with the length scale  $L$  and now the derived velocity scale  $U$ , a time scale  $T$  may be determined by examining the scaling of the mass equation (2.4)

$$\frac{H}{T} \frac{\partial \tilde{h}}{\partial t} + \frac{HU}{L} \nabla \cdot (\tilde{h} \tilde{\mathbf{u}}) = 0 \quad (3.9)$$

For the two terms of the scaled mass equation to be comparable we require

$$\frac{1}{T} = \frac{U}{L} \quad (3.10)$$

i.e.

$$T = \frac{L}{U} \quad (3.11)$$

and this completes the specifications for the scale factors.

In the computer code that was developed to produce the results shown later in this work, values for  $L$ ,  $H$ ,  $H_0$  and the Earth's rotation rate  $\Omega = F/2$  were set to typical values for synoptic scale atmospheric dynamics

$$L = 6.3675 \times 10^6 [m] \quad (3.12)$$

$$H_0 = 2.0 \times 10^3 [m] \quad (3.13)$$

$$H = 5.0 \times 10^3 [m] \quad (3.14)$$

$$\Omega = 7.292115 \times 10^{-5} [s^{-1}] \quad (3.15)$$

leading to derived values for the dependent scales of

$$\begin{aligned} U &= gH/(2\Omega L) \approx 52.82 [m/s] \\ T &= L/U \approx 33.5 [hours] \end{aligned} \quad (3.16)$$

## Spherical Coordinates

As indicated in the introduction, the governing shallow water equations are to be solved on the surface of a sphere. The coordinates of any point on the surface of such a sphere are naturally most easily expressed in terms of a spherical coordinate system  $(r, \lambda, \theta)$ . If the spherical surface is intended to represent the surface of the Earth, then  $\lambda$  corresponds to the longitude, positive east of Greenwich,  $\theta$  the latitude, positive north of the Equator, and  $r$  refers to a coordinate increasing with height above the Earth's surface.

For the two-dimensional case of the equations being solved here, variations in the direction given by this latter coordinate are neglected. Furthermore, in the spherical coordinate framework, the Coriolis term of the governing equations simply reads  $f = 2\Omega \sin \theta$ .

Adopting the standard right-handed spherical to cartesian coordinate transformation

$$x = r \cos \theta \cos \lambda \quad (4.1)$$

$$y = r \cos \theta \sin \lambda \quad (4.2)$$

$$z = r \sin \theta \quad (4.3)$$

the spherical unit direction vectors may be written in terms of their cartesian counterparts and a transformation matrix  $T$  as

$$\begin{bmatrix} \mathbf{e}_r \\ \mathbf{e}_\lambda \\ \mathbf{e}_\theta \end{bmatrix} = \overbrace{\begin{bmatrix} \cos \theta \cos \lambda & \cos \theta \sin \lambda & \sin \theta \\ -\sin \lambda & \cos \lambda & 0 \\ -\sin \theta \cos \lambda & -\sin \theta \sin \lambda & \cos \theta \end{bmatrix}}^{T^{-1}} \begin{bmatrix} \mathbf{e}_x \\ \mathbf{e}_y \\ \mathbf{e}_z \end{bmatrix} \quad (4.4)$$

and similarly, by inversion of the transformation matrix, the cartesian unit direction vectors may be given in terms of those for the spherical coordinate system

$$\begin{bmatrix} \mathbf{e}_x \\ \mathbf{e}_y \\ \mathbf{e}_z \end{bmatrix} = \overbrace{\begin{bmatrix} \cos \theta \cos \lambda & -\sin \lambda & -\sin \theta \cos \lambda \\ \cos \theta \sin \lambda & \cos \lambda & -\sin \lambda \sin \theta \\ \sin \theta & 0 & \cos \theta \end{bmatrix}}^T \begin{bmatrix} \mathbf{e}_r \\ \mathbf{e}_\lambda \\ \mathbf{e}_\theta \end{bmatrix} \quad (4.5)$$

With square braces enclosing terms that vanish for variables confined to the surface of a sphere, where all vectors are tangential to the surface, and the gradient operator in cartesian and spherical coordinates is defined as

$$\nabla = \frac{\partial}{\partial x} \mathbf{e}_x + \frac{\partial}{\partial y} \mathbf{e}_y + \frac{\partial}{\partial z} \mathbf{e}_z \quad (4.6)$$

$$= \left[ \frac{\partial}{\partial r} \mathbf{e}_r \right] + \frac{1}{r \cos \theta} \frac{\partial}{\partial \lambda} \mathbf{e}_\lambda + \frac{1}{r} \frac{\partial}{\partial \theta} \mathbf{e}_\theta \quad (4.7)$$

Similarly, the Laplacian is given by

$$\nabla^2 = \frac{\partial^2}{\partial x^2} + \frac{\partial^2}{\partial y^2} + \frac{\partial^2}{\partial z^2} \quad (4.8)$$

$$= \left[ \frac{\partial^2}{\partial r^2} \right] + \left[ \frac{2}{r} \frac{\partial}{\partial r} \right] + \frac{1}{r^2 \cos^2 \theta} \frac{\partial^2}{\partial \lambda^2} + \frac{1}{r^2} \frac{\partial^2}{\partial \theta^2} - \frac{\tan \theta}{r^2} \frac{1}{r} \frac{\partial}{\partial \theta} \quad (4.9)$$

and the divergence by

$$\nabla \cdot \mathbf{a} = \frac{\partial a_x}{\partial x} + \frac{\partial a_y}{\partial y} + \frac{\partial a_z}{\partial z} \quad (4.10)$$

$$= \left[ \frac{\partial a_r}{\partial r} \right] + \frac{1}{r \cos \theta} \frac{\partial a_\lambda}{\partial \lambda} + \frac{1}{r} \frac{\partial a_\theta}{\partial \theta} + \left[ \frac{2}{r} a_r \right] - \frac{\tan \theta}{r} a_\theta \quad (4.11)$$

The terms proportional to  $1/r$  give rise to what are often called ‘curvature terms’ when these expressions are used in the governing equations because they arise due to the curvature of the earth [15]. These terms can be important where there is a combination of both high latitudes and strong atmospheric flows.

It will be useful to consider those derivatives of the normalised spherical basis vectors with non-trivial results. With respect to  $\lambda$

$$\begin{aligned} \frac{\partial}{\partial \lambda} \begin{bmatrix} \mathbf{e}_r \\ \mathbf{e}_\lambda \\ \mathbf{e}_\theta \end{bmatrix} &= \begin{bmatrix} -\cos \theta \sin \lambda & \cos \theta \cos \lambda & 0 \\ -\cos \lambda & -\sin \lambda & 0 \\ \sin \theta \sin \lambda & -\sin \theta \cos \lambda & 0 \end{bmatrix} [T] \begin{bmatrix} \mathbf{e}_r \\ \mathbf{e}_\lambda \\ \mathbf{e}_\theta \end{bmatrix} \\ &= \begin{bmatrix} 0 & \cos \theta & 0 \\ -\cos \theta & 0 & \sin \theta \\ 0 & -\sin \theta & 0 \end{bmatrix} \begin{bmatrix} \mathbf{e}_r \\ \mathbf{e}_\lambda \\ \mathbf{e}_\theta \end{bmatrix} \end{aligned} \quad (4.12)$$

and then  $\theta$

$$\begin{aligned} \frac{\partial}{\partial \theta} \begin{bmatrix} \mathbf{e}_r \\ \mathbf{e}_\lambda \\ \mathbf{e}_\theta \end{bmatrix} &= \begin{bmatrix} -\sin \theta \cos \lambda & -\sin \theta \sin \lambda & \cos \theta \\ 0 & 0 & 0 \\ -\cos \theta \cos \lambda & -\cos \theta \sin \lambda & -\sin \theta \end{bmatrix} [T] \begin{bmatrix} \mathbf{e}_r \\ \mathbf{e}_\lambda \\ \mathbf{e}_\theta \end{bmatrix} \\ &= \begin{bmatrix} 0 & 0 & 1 \\ 0 & 0 & 0 \\ -1 & 0 & 0 \end{bmatrix} \begin{bmatrix} \mathbf{e}_r \\ \mathbf{e}_\lambda \\ \mathbf{e}_\theta \end{bmatrix} \end{aligned} \quad (4.13)$$

Finally, we will need to consider the forcing term

$$\begin{aligned} \int \nabla a \, d\lambda d\theta &= \int \left\{ \frac{1}{r \cos \theta} \frac{\partial}{\partial \lambda} \mathbf{e}_\lambda + \frac{1}{r} \frac{\partial}{\partial \theta} \mathbf{e}_\theta \right\} r^2 \cos \theta \, d\lambda d\theta \\ &= R \int \left\{ \frac{\partial}{\partial \lambda} \mathbf{e}_\lambda + \cos \theta \frac{\partial}{\partial \theta} \mathbf{e}_\theta \right\} d\lambda d\theta \end{aligned} \quad (4.14)$$

and the non-linear term of the momentum equation

$$\begin{aligned} \int \nabla \cdot \mathbf{a} \, d\lambda d\theta &= \int \left\{ \frac{1}{r \cos \theta} \frac{\partial a_\lambda}{\partial \lambda} + \frac{1}{r} \frac{\partial a_\theta}{\partial \theta} - \frac{\tan \theta}{r} a_\theta \right\} r^2 \cos \theta \, d\lambda d\theta \\ &= R \int \left\{ \frac{\partial a_\lambda}{\partial \lambda} + \cos \theta \frac{\partial a_\theta}{\partial \theta} - \sin \theta a_\theta \right\} d\lambda d\theta \end{aligned}$$

and note that

$$\mathbf{k} \times (a_\lambda \mathbf{e}_\lambda + a_\theta \mathbf{e}_\theta) = \mathbf{e}_r \times (a_\lambda \mathbf{e}_\lambda + a_\theta \mathbf{e}_\theta) = a_\lambda \mathbf{e}_\theta - a_\theta \mathbf{e}_\lambda \quad (4.15)$$

## Weak Formulations

For the mixed formulations of the shallow water equations, where both a velocity and an elevation field need to be discretized, there are two alternative weak formulations that may be found by integrating by parts different terms within either the governing mass (2.4) or momentum (2.3) equation after an appropriate arbitrary testing function has been integrated in [12].

For the momentum equation we would have

$$\int_{\Omega} \frac{D\mathbf{u}}{Dt} \cdot \hat{\mathbf{u}} \, d\tau + f \int_{\Omega} \mathbf{k} \times \mathbf{u} \cdot \hat{\mathbf{u}} \, d\tau = -g \int_{\Omega} \nabla (h + h_0) \cdot \hat{\mathbf{u}} \, d\tau \quad (5.1)$$

while for the mass equation there is

$$\int_{\Omega} \frac{\partial h}{\partial t} \hat{h} \, d\tau + \int_{\Omega} \nabla \cdot (h\mathbf{u}) \hat{h} \, d\tau = 0 \quad (5.2)$$

The choice of which weak formulation to use usually depends on the continuity requirements they place on the pre-defined basis functions associated with the velocity and elevation variables.

## Continuous Elevation Form

Now, the only term in these equations requiring continuity of the velocity field is the divergence term of the mass conservation equation. Integrating this term by parts will allow the continuity requirement to be shifted onto the elevation field, which otherwise needs to be continuous for the gradient term of the momentum equation

$$\int_{\Omega} \frac{\partial h}{\partial t} \hat{h} \, d\tau + \oint_{\partial\Omega} h \mathbf{u} \cdot \mathbf{n} \hat{h} \, ds - \int_{\Omega} h \mathbf{u} \cdot \nabla \hat{h} \, d\tau = 0 \quad (5.3)$$

## Continuous Velocity Form

Alternatively, it is the gradient term of the momentum equation which may be integrated by parts to move all the continuity constraints onto the velocity field

$$\begin{aligned} \int_{\Omega} \frac{D\mathbf{u}}{Dt} \cdot \hat{\mathbf{u}} \, d\tau + f \int_{\Omega} \mathbf{k} \times \mathbf{u} \cdot \hat{\mathbf{u}} \, d\tau \\ = -g \oint_{\partial\Omega} (h + h_0) \hat{\mathbf{u}} \cdot \mathbf{n} \, ds + g \int_{\Omega} (h + h_0) \nabla \cdot \hat{\mathbf{u}} \, d\tau \end{aligned} \quad (5.4)$$

## Boundary Terms

Of course, for global models of the atmosphere there are no physical lateral boundaries to be concerned with, however, differing versions of the equations to be discretized can be found by considering the treatment of such boundaries in more general problems.

One of the key features of weak formulations is the imposition of boundary conditions in an average, or weak sense, which has been shown to be preferable to a strong enforcement [13], [28]. For present purposes, that means removing the integrals of  $\mathbf{u} \cdot \mathbf{n}$  and  $\nabla \mathbf{u} \cdot \mathbf{n}$  on the domain boundary -the latter will be seen to arise in considerations of the viscous term.

Thus, if the boundary terms of equations (5.3) and (5.4) are not to be modelled explicitly, then different requirements need to be placed on the functional spaces from which  $\hat{h}$  and  $\hat{\mathbf{u}}$  are drawn.

If a discontinuous velocity field is to be allowed, then the continuous elevation weak form is required. Given by equations (5.1) and (5.3), the boundary integral involves the generic problem solution  $\mathbf{u}$  and may be neglected either by assuming the integrand is zero for the whole boundary (implying a strong boundary condition,  $\mathbf{u} \cdot \mathbf{n} = 0$ ), or that only the integral itself is zero -non-zero contributions from different parts of the boundary cancelling out.

Thus,  $\mathbf{u}$  may be taken from either of  $\mathcal{U}$  (strong) or  $\mathcal{U}^w$  (weak) respectively (see symbol index), the elevation  $h$  having no constraints placed on it by the boundary terms and so may be taken from  $\mathcal{H}$ .

However, should discontinuity of the elevation field be required, the boundary term of the continuous velocity weak formulation, given by equations (5.2) and (5.4), involves  $\hat{\mathbf{u}}$  and thus to be neglected requires  $\hat{\mathbf{u}} \cdot \mathbf{n} = \mathbf{0}$  for the whole boundary. This necessitates  $\mathbf{u} \in \mathcal{U}$ , with  $h \in \mathcal{H}$  again.

### Eulerian Non-linear Simplification

For Eulerian formulations, the following expression for the divergence of a dyadic,

$$\nabla \cdot (\mathbf{ab}) = (\nabla \cdot \mathbf{a}) \mathbf{b} + \mathbf{a} \cdot \nabla \mathbf{b} \quad (5.5)$$

may be used to expand the non-linear term inherent to the material derivative as

$$\mathbf{u} \cdot \nabla \mathbf{u} = \nabla \cdot (\mathbf{uu}) - \mathbf{u} \nabla \cdot \mathbf{u} \quad (5.6)$$

Integrating the momentum equation (5.1) over an arbitrary volume  $\Omega$  with this new expansion for the non-linear term

$$\begin{aligned} \int_{\Omega} \left\{ \frac{\partial \mathbf{u}}{\partial t} + \nabla \cdot (\mathbf{uu}) - \mathbf{u} \nabla \cdot \mathbf{u} + f \mathbf{k} \times \mathbf{u} \right\} \cdot \hat{\mathbf{u}} \, d\tau \\ = \int_{\Omega} -g \nabla (h + h_0) \cdot \hat{\mathbf{u}} \, d\tau \end{aligned} \quad (5.7)$$

and using the divergence theorem as applied to a dyadic

$$\int_{\Omega} \nabla \cdot (\mathbf{ab}) \, d\tau = \oint_{\partial\Omega} \mathbf{n} \cdot (\mathbf{ab}) \, ds \quad (5.8)$$

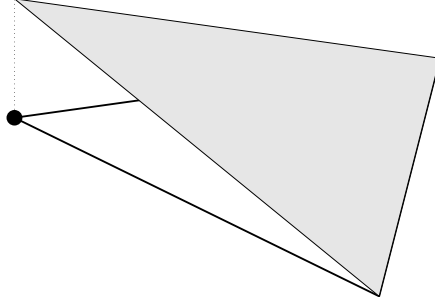


Figure 2: Linear Conforming Basis Function over Triangular Finite Element

allows the non-linear contribution to be formed

$$\int_{\Omega} \left\{ \frac{\partial \mathbf{u}}{\partial t} - \mathbf{u} \nabla \cdot \mathbf{u} + f \mathbf{k} \times \mathbf{u} \right\} \cdot \hat{\mathbf{u}} \, d\tau + \oint_{\partial\Omega} (\mathbf{u} \cdot \mathbf{n}) \mathbf{u} \cdot \hat{\mathbf{u}} \, ds = \int_{\Omega} -g \nabla (h + h_0) \cdot \hat{\mathbf{u}} \, d\tau \quad (5.9)$$

## Finite Element Spatial Discretization

To derive the finite element discretization of the governing equations, we first introduce a discretization of the domain  $\Omega$  into triangles  $\Omega_e$  ( $1 \leq e \leq N_E$ ). This triangulation is composed of  $N_{\Gamma}$  interelement segments  $\Gamma_l = \partial\Omega_e \cap \partial\Omega_f$  with  $e > f$ . Each  $\Gamma_l$  is associated with a unique normal vector  $\mathbf{n}$  which points from  $\Omega_e$  to  $\Omega_f$ . The total number of segments and vertices in the triangulation are respectively denoted  $N_S$  and  $N_V$ .

Discrete finite element equations are then found by approximating the elevation and velocity fields by summations of linear conforming,  $P_1$ , and linear non-conforming,  $P_1^{NC}$ , basis functions respectively.

### Linear Conforming Basis Functions

The three linear conforming basis functions for the canonical triangular element are given by

$$\phi_1(\xi, \eta) = 1 - \xi - \eta \quad (6.1)$$

$$\phi_2(\xi, \eta) = \xi \quad (6.2)$$

$$\phi_3(\xi, \eta) = \eta \quad (6.3)$$

where it should be noted

$$\phi_1 + \phi_2 + \phi_3 = 1 \quad (6.4)$$

One such basis function may be seen for the general triangular finite element in Figure 2.

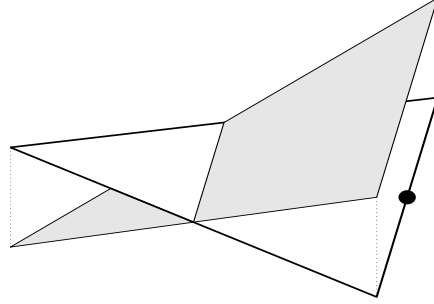


Figure 3: Linear Non-Conforming Basis Function over Triangular Finite Element

The mass matrix for the canonical triangular element, of area  $A = 1/2$ , on which these basis functions are defined is dense and fully populated

$$M = \begin{bmatrix} \langle \phi_1 \phi_1 \rangle & \langle \phi_1 \phi_2 \rangle & \langle \phi_1 \phi_3 \rangle \\ \langle \phi_2 \phi_1 \rangle & \langle \phi_2 \phi_2 \rangle & \langle \phi_2 \phi_3 \rangle \\ \langle \phi_3 \phi_1 \rangle & \langle \phi_3 \phi_2 \rangle & \langle \phi_3 \phi_3 \rangle \end{bmatrix} = \frac{A}{12} \begin{bmatrix} 2 & 1 & 1 \\ 1 & 2 & 1 \\ 1 & 1 & 2 \end{bmatrix} \quad (6.5)$$

where

$$\langle \phi_i \phi_j \rangle = \int_{\xi=0}^1 \int_{\eta=0}^{1-\xi} \phi_i \phi_j \, d\tau \quad (6.6)$$

### Linear Non-Conforming Basis Functions

Similarly, the linear non-conforming basis functions defined on the same canonical triangular element, one of which can be seen in Figure 3, are given by

$$\psi_1(\xi, \eta) = 2(\xi + \eta) - 1 \quad (6.7)$$

$$\psi_2(\xi, \eta) = 1 - 2\xi \quad (6.8)$$

$$\psi_3(\xi, \eta) = 1 - 2\eta \quad (6.9)$$

again with a summation to unity

$$\psi_1 + \psi_2 + \psi_3 = 1 \quad (6.10)$$

However, a major advantage of the non-conforming basis functions is the following orthogonality property

$$\int_T \psi_i \psi_j \, d\tau = \frac{A}{3} \delta_{ij} \quad (6.11)$$

where  $A = 1/2$  again corresponds to the area of the canonical element.

Thus, the elemental mass matrix using these basis functions is diagonal

$$N = \begin{bmatrix} \langle \psi_1 \psi_1 \rangle & \langle \psi_1 \psi_2 \rangle & \langle \psi_1 \psi_3 \rangle \\ \langle \psi_2 \psi_1 \rangle & \langle \psi_2 \psi_2 \rangle & \langle \psi_2 \psi_3 \rangle \\ \langle \psi_3 \psi_1 \rangle & \langle \psi_3 \psi_2 \rangle & \langle \psi_3 \psi_3 \rangle \end{bmatrix} = \frac{A}{3} \begin{bmatrix} 1 & 0 & 0 \\ 0 & 1 & 0 \\ 0 & 0 & 1 \end{bmatrix} \quad (6.12)$$

with the  $\langle \rangle$  operator defined as before.

### Summations

Thus we may let the unknown elevation field be represented by the following summation

$$h = h(\lambda, \theta) \approx h^h(\lambda, \theta) = \sum_{j=1}^{N_V} h_j \phi_j(\lambda, \theta) \quad (6.13)$$

and similarly the unknown velocity (vector) field by the summation

$$\mathbf{u} = \mathbf{u}(\lambda, \theta) \approx \mathbf{u}^h(\lambda, \theta) = \sum_{j=1}^{N_S} \mathbf{u}_j \psi_j(\lambda, \theta) = \sum_{j=1}^n \{u_j \psi_j \mathbf{e}_\lambda + v_j \psi_j \mathbf{e}_\theta\} \quad (6.14)$$

The conforming and non-conforming shape functions  $\phi_j$  and  $\psi_j$  have the same expressions as before except that now they linearly depend on the spherical coordinates  $\lambda$  and  $\theta$ .

### Testing the Continuous Elevation Weak Formulation

Following a discontinuous Galerkin procedure, the discretized expressions (6.14) and (6.13) may now be substituted into the equations of the continuous elevation weak formulation (5.9) and (5.3) with computational regions taken to be each triangle  $\Omega_e$  of the finite element discretization in turn, with the testing functions  $\hat{\mathbf{u}}$  and  $\hat{h}$  drawn from the same set as used for the respective discretizations.

### Momentum Equation

Starting with the momentum equation (5.9) and taking repeated indices to indicate summation over the full index range

$$\begin{aligned} & \int_{\Omega_e} \frac{\partial \overbrace{(\mathbf{u}_j \psi_j)}^{\mathbf{u}^h}}{\partial t} \cdot \mathbf{1} \psi_i \, d\tau - \int_{\Omega_e} \nabla \cdot (\mathbf{u}_k \psi_k) [\mathbf{u}_j \psi_j] \cdot \mathbf{1} \psi_i \, d\tau \\ & + \oint_{\partial\Omega_e} (\mathbf{u}^h \cdot \mathbf{n}) [\mathbf{u}_j \psi_j] \cdot \mathbf{1} \psi_i \, ds + \mathbf{k} \times \mathbf{u}_j \cdot \mathbf{1} \int_{\Omega_e} f \psi_i \psi_j \, d\tau \\ & = -h_j g \int_{\Omega_e} \nabla \phi_j \cdot \mathbf{1} \psi_i \, d\tau - g \int_{\Omega_e} \nabla h_0 \cdot \mathbf{1} \psi_i \, d\tau \end{aligned} \quad (7.1)$$

where  $\mathbf{1} = \mathbf{e}_\lambda + \mathbf{e}_\theta$ .

Identifying the two spherical components of  $\mathbf{u}_j = u_j \mathbf{e}_\lambda + v_j \mathbf{e}_\theta$  explicitly, the two scalar momentum equations may be formed by considering the  $\mathbf{e}_\lambda$  and  $\mathbf{e}_\theta$  components of the testing vector  $\mathbf{1}$ . Testing the zonal ( $\lambda$ ) component with  $\mathbf{e}_\lambda$  and

using the expression for the gradient operator (4.7) gives

$$\begin{aligned} & \frac{du_j}{dt} \int_{\Omega_e} \psi_i \psi_j \, d\tau - \int_{\Omega_e} \nabla \cdot \overbrace{(\mathbf{u}_k \psi_k)}^{\mathbf{u}^h} \overbrace{[u_j \psi_j]}^{u^h} \psi_i \, d\tau - v_j \int_{\Omega_e} f \psi_i \psi_j \, d\tau \\ & + \oint_{\partial\Omega_e} \overbrace{\left[ \frac{\partial \mathbf{u}^h}{\partial n} \right]}^{\text{upwind}} \psi_i \overbrace{[u_j \psi_j]}^{u^h} \, ds = - (h_j + h_{0j}) \, g \int_{\Omega_e} \frac{1}{r \cos \theta} \frac{\partial \phi_j}{\partial \lambda} \psi_i \, d\tau \end{aligned} \quad (7.2)$$

while testing the meridional ( $\theta$ ) component with  $\mathbf{e}_\theta$  returns

$$\begin{aligned} & \frac{dv_j}{dt} \int_{\Omega_e} \psi_i \psi_j \, d\tau - \int_{\Omega_e} \nabla \cdot \overbrace{(\mathbf{u}_k \psi_k)}^{\mathbf{u}^h} \overbrace{[v_j \psi_j]}^{v^h} \psi_i \, d\tau + u_j \int_{\Omega_e} f \psi_i \psi_j \, d\tau \\ & + \oint_{\partial\Omega_e} \overbrace{\left[ \frac{\partial \mathbf{u}^h}{\partial n} \right]}^{\text{upwind}} \psi_i \overbrace{[v_j \psi_j]}^{v^h} \, ds = - (h_j + h_{0j}) \, g \int_{\Omega_e} \frac{1}{r} \frac{\partial \phi_j}{\partial \theta} \psi_i \, d\tau \end{aligned} \quad (7.3)$$

where the normal derivatives and approximations to zonal  $u^h$  and meridional  $v^h$  velocities appearing in the integrals over the boundary of the finite element  $\partial\Omega_e$  need to be upwinded in the manner described below and where we have noted

$$\begin{aligned} \mathbf{k} \times \mathbf{u}_j \cdot \mathbf{1} &= \{ \mathbf{e}_r \times [u_j \mathbf{e}_\lambda + v_j \mathbf{e}_\theta] \} \cdot (\mathbf{e}_\lambda + \mathbf{e}_\theta) \\ &= [u_j \mathbf{e}_\theta - v_j \mathbf{e}_\lambda] \cdot (\mathbf{e}_\lambda + \mathbf{e}_\theta) \\ &= u_j - v_j \end{aligned} \quad (7.4)$$

Introducing the actual differentials for the triangular computational domains of each finite element, now labeled  $\Omega_e$ , such that  $d\tau = a^2 \cos \theta d\lambda d\theta$  and using the spherical polar expression for the divergence operator (4.11) we obtain

$$\begin{aligned} & \frac{du_j}{dt} \overbrace{a^2 \int_{\Omega_e} \psi_i \psi_j \cos \theta \, d\lambda d\theta}^{m_{ij}} + \oint_{\partial\Omega_e} \overbrace{\left[ \frac{\partial \mathbf{u}^h}{\partial n} \right]}^{\text{upwind}} \overbrace{[u^h]}^{\text{upwind}} \psi_i \, ds - u_j u_k \, a \int_{\Omega_e} \psi_i \psi_j \frac{\partial \psi_k}{\partial \lambda} \, d\lambda d\theta \\ & - u_j v_k \, a \int_{\Omega_e} \psi_i \psi_j \frac{\partial \psi_k}{\partial \theta} \cos \theta \, d\lambda d\theta + u_j v_k \, a \int_{\Omega_e} \psi_i \psi_j \psi_k \sin \theta \, d\lambda d\theta \\ & - v_j \, a^2 \int_{\Omega_e} f \psi_i \psi_j \cos \theta \, d\lambda d\theta = -g \, (h_j + h_{0j}) \, a \int_{\Omega_e} \psi_i \frac{\partial \phi_j}{\partial \lambda} \, d\lambda d\theta \end{aligned} \quad (7.5)$$

for the zonal component, and

$$\begin{aligned} \frac{dv_j}{dt} & \overbrace{a^2 \int_{\Omega_e} \psi_i \psi_j \cos \theta \, d\lambda d\theta}^{m_{ij}} + \oint_{\partial\Omega_e} \overbrace{\left[ \frac{\partial u^h}{\partial n} \right]}^{upwind} \overbrace{[v^h]}^{upwind} \psi_i \, ds - u_k v_j \, a \int_{\Omega_e} \psi_i \psi_j \frac{\partial \psi_k}{\partial \lambda} \, d\lambda d\theta \\ & - v_j v_k \, a \int_{\Omega_e} \psi_i \psi_j \frac{\partial \psi_k}{\partial \theta} \cos \theta \, d\lambda d\theta + v_j v_k \, a \int_{\Omega_e} \psi_i \psi_j \psi_k \sin \theta \, d\lambda d\theta \\ & + u_j \, a^2 \int_{\Omega_e} f \psi_i \psi_j \cos \theta \, d\lambda d\theta = -g \, (h_j + h_{0j}) \, a \int_{\Omega_e} \psi_i \frac{\partial \phi_j}{\partial \theta} \cos \theta \, d\lambda d\theta \end{aligned} \quad (7.6)$$

for the meridional. The  $m_{ij}$  label, corresponding to the coefficient for the time derivatives in the momentum equations will be used later.

If the summations of both of the last two equations are considered over all elements  $\Omega_e$  of the computational domain, then ‘right hand side’ terms may be generated for either equation from the collection of terms that will be handled explicitly

$$m_{ii} \frac{\partial u_i}{\partial t} = b_u \quad (7.7)$$

$$m_{ii} \frac{\partial v_i}{\partial t} = b_v \quad (7.8)$$

where due to the orthogonality of the non-conforming linear basis functions, the coefficients  $m_{ij}$  for the time derivatives in the two discretized momentum equations (7.5) and (7.6), are non-zero only when the testing and interpolation functions are the same,  $m_{ij} = 0$  if  $i \neq j$ , giving rise to a diagonal velocity mass matrix  $m_{ij}$ .

Note that the non-linear terms have been integrated by parts to get fluxes between elements. These fluxes need to be discretized in an upwind fashion by adding some continuity constraints to the equations as will be explained in the next but one sub-section.

## Mass Equation

Similarly testing the mass conservation equation (5.3) with the linear conforming basis function,  $\phi_i$ , to be used for the elevation

$$\frac{\partial h_j}{\partial t} \int_{\Omega} \phi_i \phi_j \, d\tau - \int_{\Omega} [h_j \phi_j] \left( u_j \psi_j \frac{1}{r \cos \theta} \frac{\partial \phi_i}{\partial \lambda} + v_j \psi_j \frac{1}{r} \frac{\partial \phi_i}{\partial \theta} \right) \, d\tau = 0 \quad (7.9)$$

Now introducing the specific differentials associated with integration over the triangular finite element  $\Omega_e$

$$\begin{aligned} \frac{\partial h_j}{\partial t} & \overbrace{a^2 \int_{\Omega_e} \phi_i \phi_j \cos \theta \, d\lambda d\theta}^{n_{ij}} - u_j h_j \, a \int_{\Omega_e} \frac{\partial \phi_i}{\partial \lambda} \phi_j \psi_j \, d\lambda d\theta \\ & - v_j h_j \, a \int_{\Omega_e} \frac{\partial \phi_i}{\partial \theta} \phi_j \psi_j \cos \theta \, d\lambda d\theta = 0 \end{aligned} \quad (7.10)$$

where a comparable notation of  $n_{ij}$  has been used for the coefficient of the time derivative for the mass equation.

Again, accumulating all such integrals over elements of the computational domain allows us to introduce the right hand side term  $b_h$

$$n_{ii} \frac{\partial h_i}{\partial t} = b_h \quad (7.11)$$

where to achieve the same simple structure for the elevation mass equation (7.10), given that the conforming basis functions used for the elevation field are *not* orthogonal, the equivalent mass matrix needs to be lumped, with all its off-diagonal terms ‘lumped’ to the diagonal  $n_{ii} \neq 0$ . Fortunately, for the fast gravity and slow Rossby waves we might expect in the synoptic scale atmospheric dynamics we are interested in, the effects of such lumping on the dispersion of such waves is limited [19].

## Time Discretization

Time derivatives are discretized with an explicit 3rd-Order Adams-Bashforth scheme. This has been shown to be superior to the other commonly employed explicit ‘Leapfrog’ scheme, because it is stable even when there is a small amount of diffusion present (a necessary requirement for some calculations as will be seen) whilst similarly requiring just one evaluation of the right hand side coefficients per iteration [9]. This method will be applied to the standard forms of equations (7.7), (7.8) and (7.11).

With the lumped fully diagonal system for the time derivatives of the unknown velocities and elevation, and all the remaining terms of the equations handled explicitly, contributing solely to a forcing vector  $\mathbf{b} = (\mathbf{b}_u, \mathbf{b}_v, \mathbf{b}_h)$ , where  $\mathbf{b}_u$ ,  $\mathbf{b}_v$  and  $\mathbf{b}_h$  refer to the right hand sides of the two momentum and mass equations respectively with only the time derivatives on the left hand side to be solved for, then the following explicit third-order Adams-Bashforth scheme may be used

$$\begin{bmatrix} \mathbf{U} \\ \mathbf{V} \\ \mathbf{H} \end{bmatrix}^{n+1} = \begin{bmatrix} \mathbf{U} \\ \mathbf{V} \\ \mathbf{H} \end{bmatrix}^n + \frac{\Omega_e t}{12 \{m_{ii}|n_{ii}\}} \left\{ 23 \begin{bmatrix} \mathbf{b}_u \\ \mathbf{b}_v \\ \mathbf{b}_h \end{bmatrix}^n - 16 \begin{bmatrix} \mathbf{b}_u \\ \mathbf{b}_v \\ \mathbf{b}_h \end{bmatrix}^{n-1} + 5 \begin{bmatrix} \mathbf{b}_u \\ \mathbf{b}_v \\ \mathbf{b}_h \end{bmatrix}^{n-2} \right\} \quad (7.12)$$

where division by  $m_{ii}$  is used when updating the values of  $\{u_i\} = \mathbf{U}$  and  $\{v_i\} = \mathbf{V}$ , from time-level  $n$  to  $n + 1$ , and  $n_{ii}$  is used for updating  $\{h_i\} = \mathbf{H}$ .

## Upwinding

Having established the method by which the general velocity and elevation solutions will be found through updating from initial conditions, mention is now needed of the contribution made by the boundary integrals, over  $\partial\Omega_e$ , appearing

in equations (7.5) and (7.6). Without loss of generality, we shall consider the normal derivative term, similar arguments may be made for the other upwinded terms.

Consider the sum of two such boundary integrals appearing in the full discretized zonal momentum equation for the whole computational domain, and arising from the integrations over two neighbouring elements labelled  $i$  and  $j$  with boundaries  $\partial\Omega_i$  and  $\partial\Omega_j$  respectively.

$$\oint_{\partial\Omega_i} \frac{\partial u^h}{\partial n_i} [\dots] ds + \oint_{\partial\Omega_j} \frac{\partial u^h}{\partial n_j} [\dots] ds \quad (7.13)$$

Let the shared side between such elements be denoted by  $\Gamma_{ij}$  with the subscript order indicating the direction in which the segment is to be traversed and with a normal  $\mathbf{n}_i$  pointing away from element  $i$  into element  $j$  and a normal  $\mathbf{n}_j$  pointing away from element  $j$  into element  $i$ . Then the contributions to the last sum from this edge will be

$$\int_{\Gamma_{ij}} \frac{\partial u^h}{\partial n_i} [\dots] ds + \oint_{\Gamma_{ji}} \frac{\partial u^h}{\partial n_j} [\dots] ds \quad (7.14)$$

To avoid a spurious build up of mass along the interface between the two elements, we would expect

$$\frac{\partial u^h}{\partial n_i} = -\frac{\partial u^h}{\partial n_j} \quad (7.15)$$

considering that the normals are in opposite directions.

To enforce this continuity restraint it is necessary to decide how the different values of  $\partial u^h/\partial n$  inside each of the two elements are to contribute to this shared value. This bias may be summarised with a parameter  $\lambda$  such that the flux over the interface is given by

$$\frac{\partial u^h}{\partial n} = (1 - \lambda) \left. \frac{\partial u^h}{\partial n_i} \right|_{\Omega_{upwind}} - \lambda \left. \frac{\partial u^h}{\partial n_j} \right|_{\Omega_{downwind}} \quad (7.16)$$

where the ‘downwind’ and ‘upwind’ subscripts indicate the elements into which there is a net flow in and out of the element respectively.

There has been much work on the exact choice that should be made for this upwinding parameter. For the present work however, and with numerical stability in mind, a full upwind scheme is used. Thus the element for which the flux over the edge is positive (a net out-flow) determines the size of this flux exclusively, with no input from the solution values within the adjoining element into which the flow is arriving. This corresponds to a setting of  $\lambda = 0$  in the last equation.

It has been shown that such a fully-upwinded scheme introduces some numerical diffusion that filters out high frequency oscillations (that could otherwise pollute the solution and lead to numerical instability) by diffusing only wavelengths that are barely resolved [14]. Because of this direct influence on disturbances with

wavelengths smaller than the typical grid element dimensions, such upwinding can be seen as a sub-grid scale model [14].

## Artificial Diffusion

Although the use of non-conforming basis functions for velocity fields is known to dissipate high order oscillations within a solution [14], and even with fully upwinded equations, numerical instabilities in the solution can still set in.

In common with other investigators, [17], it was found to be necessary to introduce some artificial viscosity to ‘dampen’, and hence stabilize, the solution.

Numerical modelling of advection dominated processes has to deal with energy transport from larger to smaller physical wavelengths. Because the computational grid gives a lower limit for the discrete wavelengths [but not an upper limit], an energy accumulation in the small scales can lead to numerical instabilities [17]

These instabilities are thus triggered by the attempted propagation of wavelengths too small to be modelled adequately with the given mesh resolution, arising from energy transport from larger scales.

It should be noted that small scale features, either in the solution itself, such as the steep geopotential gradients associated with highly sheared flows, or in the problem description, such as small topographic obstacles, can also generate disturbances with such poorly resolved wavelengths.

Thus, in the preliminary experiments for the work reported here, it was found expedient to introduce an artificial viscosity into the solution in order to erode some of these local velocity extrema, and dissipate some of the energy accumulated in the smaller scales.

With the molecular diffusion of air roughly  $10^{-5} \text{ m}^2/\text{s}$ , the typical viscosity parameter  $\nu$  used, where stated, in the computations of the results, was chosen to be more representative of an eddy viscosity  $10^{11}$  times greater at  $10^6 \text{ m}^2/\text{s}$ .

The diffusion term appearing in square brackets in equation (2.1), to be handled completely explicitly to preserve the efficiency of the numerical scheme, is thus added to the right hand side of equation (7.1). Before examining its exact form, however, it should be noted that in the following

$$\nabla \mathbf{u} = \nabla (u \mathbf{e}_\lambda + v \mathbf{e}_\theta) \quad (7.17)$$

will refer to a dyadic and will be used with the dyadic identity

$$\nabla \cdot (\phi \mathbf{A}) = \nabla \phi \cdot \mathbf{A} + \phi \nabla \cdot \mathbf{A} \quad (7.18)$$

where  $\phi$  refers to a general scalar quantity, and  $\mathbf{A}$  refers to a general dyadic, and also the dyadic integral divergence identity

$$\int_V \nabla \cdot \mathbf{A} \, d\tau = \int_S \mathbf{n} \cdot \mathbf{A} \, ds \quad (7.19)$$

where the volume  $V$  is bounded by the surface  $S$ .

The general (vector) diffusion term used to smooth the solution and act against the creation of local velocity extrema was shown to be

$$E_k \frac{1}{\tilde{h}} \tilde{\nabla} \cdot (\tilde{h} \tilde{\nabla} \tilde{\mathbf{u}}) \quad (7.20)$$

in the dimensionless form of the momentum equation (3.3).

With this non-dimensional form now being understood (and the tildes neglected), we may now test this new term in the manner outlined above, by integrating in the vector test function  $\psi_i \mathbf{1}$  over the computational domain of each individual finite element  $\Omega_e$  separately, allowing an application of the dyadic divergence identity that introduces the local momentum fluxes over the edges of the elements

$$\begin{aligned} & \int_{\Omega_e} \nu \frac{\psi_i}{h} [\nabla \cdot (h \nabla \mathbf{u})] \cdot \mathbf{1} \, d\tau \\ &= \int_{\Omega_e} \nu \left[ \nabla \cdot \left( \frac{\psi_i}{h} h \nabla \mathbf{u} \right) \right] \cdot \mathbf{1} \, d\tau - \int_{\Omega_e} \nu \nabla \left( \frac{\psi_i}{h} \right) \cdot (h \nabla \mathbf{u}) \cdot \mathbf{1} \, d\tau \\ &= \oint_{\partial\Omega_e} \nu [\psi_i \mathbf{n} \cdot \nabla \mathbf{u}] \cdot \mathbf{1} \, ds - \int_{\Omega_e} \nu \nabla \left( \frac{\psi_i}{h} \right) \cdot (h \nabla \mathbf{u}) \cdot \mathbf{1} \, d\tau \end{aligned} \quad (7.21)$$

Now, if the dyadic flux  $\mathbf{n} \cdot \nabla \mathbf{u}$  is assumed constant over each of the three pieces of the boundary  $\partial\Omega_e$ , then the boundary integral above may be neglected. This is because of the nature of the non-conforming basis function  $\psi_i$  used to test the equation.

If  $\psi_i$  refers to either of the basis functions not uniformly equal to one on the particular segment of  $\partial\Omega_e$ , see Figure 3, then it will vary from +1 to -1 linearly across that segment. Because  $\psi_i$  appears, with the (constant) flux, in this boundary integral in the absence of any other interfering basis functions, this will allow it to remove the integral altogether.

Flux continuity over element edges and thus cancellations between the boundary integrals arising from neighbouring elements will remove the integral for the case where  $\psi_i$  is uniformly +1 over the segment. We thus need only consider the

integral over  $\Omega_e$  itself

$$\begin{aligned}
 &= -\nu \int_{\Omega_e} \left\{ \frac{1}{r \cos \theta} \frac{\partial}{\partial \lambda} \left( \frac{\psi_i}{h} \right) \mathbf{e}_\lambda + \frac{1}{r} \frac{\partial}{\partial \theta} \left( \frac{\psi_i}{h} \right) \mathbf{e}_\theta \right\} \\
 &\quad \cdot \left( h \left\{ \frac{1}{r \cos \theta} \frac{\partial}{\partial \lambda} (u \mathbf{e}_\lambda + v \mathbf{e}_\theta) \mathbf{e}_\lambda + \frac{1}{r} \frac{\partial}{\partial \theta} (u \mathbf{e}_\lambda + v \mathbf{e}_\theta) \mathbf{e}_\theta \right\} \right) \cdot \mathbf{1} \, d\tau \\
 &= -\nu \int_{\Omega_e} \left\{ \frac{1}{r \cos \theta} \left[ \frac{\partial}{\partial \lambda} \left( \frac{\psi_i}{h} \right) \right] \mathbf{e}_\lambda + \frac{1}{r} \left[ \frac{\partial}{\partial \theta} \left( \frac{\psi_i}{h} \right) \right] \mathbf{e}_\theta \right\} \\
 &\quad \cdot h \left\{ \frac{1}{r \cos \theta} \left[ \frac{\partial u}{\partial \lambda} \mathbf{e}_\lambda + u \sin \theta \mathbf{e}_\theta + \frac{\partial v}{\partial \lambda} \mathbf{e}_\theta - v \sin \theta \mathbf{e}_\lambda \right] \mathbf{e}_\lambda + \frac{1}{r} \left[ \frac{\partial u}{\partial \theta} \mathbf{e}_\lambda + \frac{\partial v}{\partial \theta} \mathbf{e}_\theta \right] \mathbf{e}_\theta \right\} \cdot \mathbf{1} \, d\tau \\
 &= -\nu \int_{\Omega_e} \frac{h}{r^2 c^2} \{ S_{,\lambda} \mathbf{e}_\lambda + c S_{,\theta} \mathbf{e}_\theta \} \cdot \{ u_{,\lambda} \mathbf{e}_\lambda \mathbf{e}_\lambda + u s \mathbf{e}_\theta \mathbf{e}_\lambda + v_{,\lambda} \mathbf{e}_\theta \mathbf{e}_\lambda - v s \mathbf{e}_\lambda \mathbf{e}_\lambda \\
 &\quad + c u_{,\theta} \mathbf{e}_\lambda \mathbf{e}_\theta + c v_{,\theta} \mathbf{e}_\theta \mathbf{e}_\theta \} \cdot (\mathbf{e}_\lambda + \mathbf{e}_\theta) \, d\tau \tag{7.22}
 \end{aligned}$$

where the derivatives of the standard spherical unit basis vectors are given by equations (4.12) and (4.13), and a compact notation has been introduced

$$c = \cos \theta; \quad s = \sin \theta; \quad S = \frac{\psi_i}{h} \tag{7.23}$$

... continuing ...

$$\begin{aligned}
 &= -\nu \int_{\Omega_e} \frac{h}{r^2 c^2} S_{,\lambda} \{ u_{,\lambda} \mathbf{e}_\lambda \cdot \mathbf{e}_\lambda \mathbf{e}_\lambda + u s \mathbf{e}_\lambda \cdot \mathbf{e}_\theta \mathbf{e}_\lambda + v_{,\lambda} \mathbf{e}_\lambda \cdot \mathbf{e}_\theta \mathbf{e}_\lambda - v s \mathbf{e}_\lambda \cdot \mathbf{e}_\lambda \mathbf{e}_\lambda \\
 &\quad + c u_{,\theta} \mathbf{e}_\lambda \cdot \mathbf{e}_\lambda \mathbf{e}_\theta + c v_{,\theta} \mathbf{e}_\lambda \cdot \mathbf{e}_\theta \mathbf{e}_\theta \} \cdot (\mathbf{e}_\lambda + \mathbf{e}_\theta) \, d\tau \\
 &\quad -\nu \int_{\Omega_e} \frac{h}{r^2 c^2} c S_{,\theta} \{ u_{,\lambda} \mathbf{e}_\theta \cdot \mathbf{e}_\lambda \mathbf{e}_\lambda + u s \mathbf{e}_\theta \cdot \mathbf{e}_\theta \mathbf{e}_\lambda + v_{,\lambda} \mathbf{e}_\theta \cdot \mathbf{e}_\theta \mathbf{e}_\lambda - v s \mathbf{e}_\theta \cdot \mathbf{e}_\lambda \mathbf{e}_\lambda \\
 &\quad + c u_{,\theta} \mathbf{e}_\theta \cdot \mathbf{e}_\lambda \mathbf{e}_\theta + c v_{,\theta} \mathbf{e}_\theta \cdot \mathbf{e}_\theta \mathbf{e}_\theta \} \cdot (\mathbf{e}_\lambda + \mathbf{e}_\theta) \, d\tau \\
 &= -\nu \int_{\Omega_e} \frac{h}{r^2 c^2} S_{,\lambda} \{ u_{,\lambda} \mathbf{e}_\lambda \cdot \mathbf{e}_\lambda - v s \mathbf{e}_\lambda \cdot \mathbf{e}_\lambda + c u_{,\theta} \mathbf{e}_\theta \cdot \mathbf{e}_\lambda \} \, d\tau \\
 &\quad -\nu \int_{\Omega_e} \frac{h}{r^2 c^2} c S_{,\theta} \{ +u s \mathbf{e}_\lambda \cdot \mathbf{e}_\lambda + v_{,\lambda} \mathbf{e}_\lambda \cdot \mathbf{e}_\lambda + c v_{,\theta} \mathbf{e}_\theta \cdot \mathbf{e}_\lambda \} \, d\tau \\
 &\quad -\nu \int_{\Omega_e} \frac{h}{r^2 c^2} S_{,\lambda} \{ u_{,\lambda} \mathbf{e}_\lambda \cdot \mathbf{e}_\theta - v s \mathbf{e}_\lambda \cdot \mathbf{e}_\theta + c u_{,\theta} \mathbf{e}_\theta \cdot \mathbf{e}_\theta \} \, d\tau \\
 &\quad -\nu \int_{\Omega_e} \frac{h}{r^2 c^2} c S_{,\theta} \{ +u s \mathbf{e}_\lambda \cdot \mathbf{e}_\theta + v_{,\lambda} \mathbf{e}_\lambda \cdot \mathbf{e}_\theta + c v_{,\theta} \mathbf{e}_\theta \cdot \mathbf{e}_\theta \} \, d\tau \\
 &= -\nu \int_{\Omega_e} \frac{h}{c} \{ (u_{,\lambda} - v s) S_{,\lambda} + (u s + v_{,\lambda}) c S_{,\theta} \} \, d\lambda d\theta \quad (\lambda) \\
 &\quad -\nu \int_{\Omega_e} \frac{h}{c} \{ c u_{,\theta} S_{,\lambda} + c v_{,\theta} c S_{,\theta} \} \, d\lambda d\theta \quad (\theta) \tag{7.24}
 \end{aligned}$$

where in the last line(s) we have introduced the specific spherical polar incremental elements and identified the contributions the new diffusion term makes to the right hand sides of the scalar equations (7.5) and (7.6) with  $(\lambda)$  and  $(\theta)$  respectively.

## Numerical Experiments

### Introduction

For the validation of the code as adapted to a spherical geometry, a number of test cases suggested by Williamson et al. [29], appropriate to the use of the shallow water equations on a sphere, was considered. These tests started from relatively simple experiments to validate the purely advective properties of the code, by resetting the winds to the initial values every timestep and observing the propagation of a Cosine Bell disturbance (test case 1), to the much more sophisticated replication of gravity waves excited by an isolated mountain (test case 5) and approximations to the Rossby-Haurwitz waves. The latter are actually analytic solutions to the non-linear barotropic vorticity equation (derived from the shallow water equations) on the sphere, but which may be approximated in the shallow water model (test case 6).

In the following, solutions for test cases 1,5,6 and 7 of [29] were generated, the last test being liberally interpreted as simply running the numerical model on a realistic data set (taken for current purposes from the ECMWF archives). The test cases 2,3 and 4 would appear to be less popular in the literature, are thus harder to find comparisons for, and are not reported here. A structured mesh generator was developed to create meshes of various different sizes (in terms of the number of elements they consisted of), with a very uniform element size distribution as can be seen in the sequence shown in Figure 4.

The largest of these structured meshes, with 20480 elements, was used to capture the dissipative processes and steep velocity gradients of test cases 1 and 5. The initial conditions of test case 1 may be seen on this mesh in Figure 5. However, a much smaller structured mesh of 8192 elements, derived from recursion of the icosahedron, was tried for the simpler test case 6 anticipating the solution's smoother behaviour.

The last test case, employing actual data, was initially tried with the larger mesh, but difficulties emerged with numerical stability (as will be discussed), even when a little artificial diffusion was allowed. A useable, if somewhat coarsely defined result was, however, obtained with the smaller mesh used for test case 6 (and a little diffusion), and those results are presented here.

Note that because the structured mesh generator was based on the recursive refinement of the triangular faces of some simple canonical geometries, namely the icos- and isos-ahedrons, significant differences in possible mesh sizes were inevitable.

### Test Case One: Pure Advection of a Cosine Bell

[This] is the only case of the suite that does not deal with the complete shallow water equations. It tests the advective component in isola-

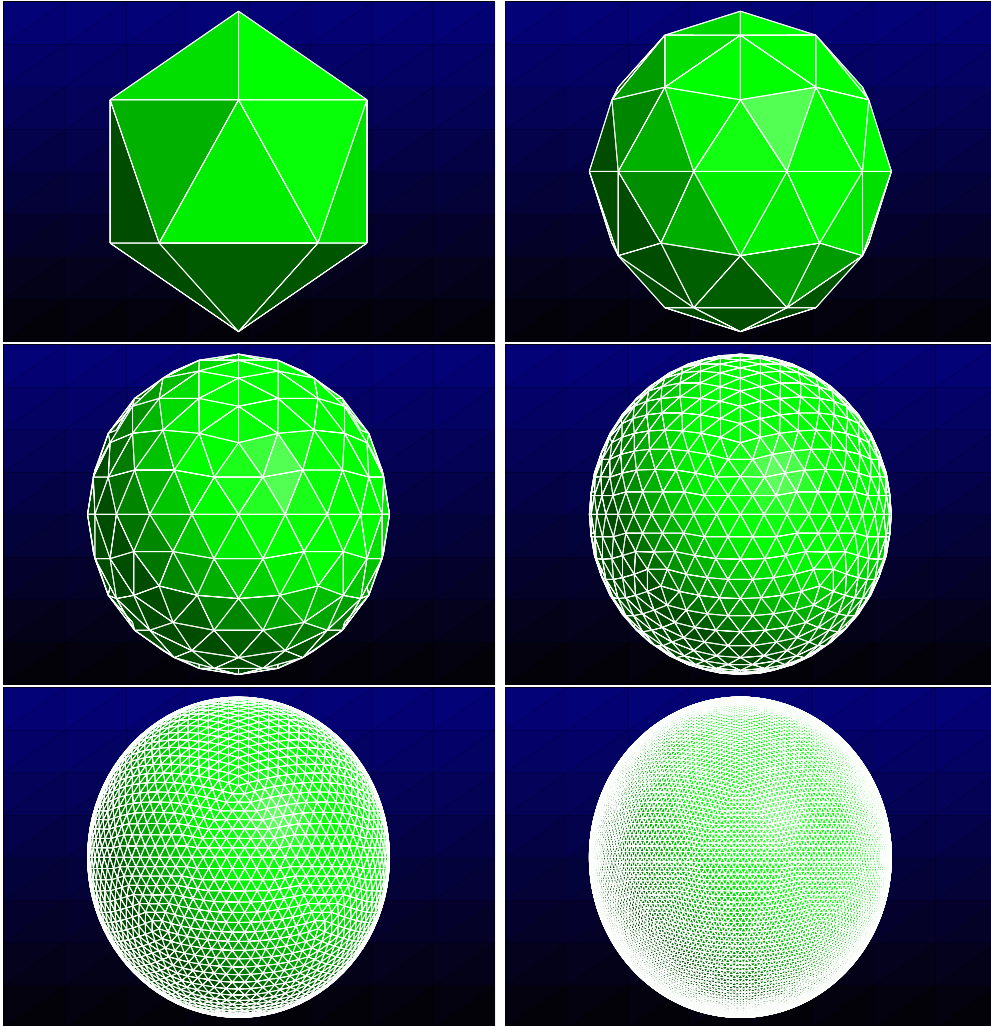


Figure 4: Structured meshes of 20, 80, 320, 1280, 5120 and 20480 elements generated by recursive refinement of the icosahedron (top left). A similar set of meshes may be generated starting from the isosahedron.

tion. Many shallow water codes can be easily changed for this test by overwriting the predicted wind field every time step with the analytically specified advecting wind. Since this wind field is non-divergent the equation for the height of the free surface reduces to the advection equation [29]

The advecting wind field for the cosine bell, that corresponds to a solid body rotation, making one complete revolution in about 12 days, is given by

$$\begin{aligned} u &= u_0 (\cos \theta \cos \alpha + \sin \theta \cos \lambda \sin \alpha) \\ v &= -u_0 \sin \lambda \sin \alpha \end{aligned} \tag{8.1}$$

where the parameter  $\alpha$  corresponds to the angle between the axis of solid body rotation and the polar axis of the spherical coordinate system and allows for the direction of advection to be varied to test the isotropy of the method and/or mesh considered [29]. For the solution presented here this is kept at zero, giving rise to an advection around the equator.

The initial cosine bell test pattern that is to be advected is given by

$$h(\lambda, \theta) = \frac{h_0}{2} \left( 1 + \cos\left(\frac{\pi r}{R}\right) \right) \quad (8.2)$$

for  $r < R$ , and  $h(\lambda, \theta) = 0$  otherwise, where  $h_0 = 1000m$  and  $r$  is the great circle distance between  $(\lambda, \theta)$  and the center of the mountain, initially taken as  $(\lambda_c, \theta_c) = (3\pi/2, 0)$ , and is given by

$$r = a \cos^{-1} [\sin \theta_c \sin \theta + \cos \theta_c \cos \theta \cos(\lambda - \lambda_c)] \quad (8.3)$$

The radius  $R = a/4$  and the advecting wind velocity is given by

$$u_0 = \frac{2 \pi a}{12 \text{ days}} \quad (8.4)$$

which corresponds to about 40 m/s. No artificial viscosity was introduced for this test case.

As can be seen in Figure 6, there appears to be a slight loss in height of the initial disturbance, and a large associated ‘dip’ behind, as it propagates around the Earth. This can be attributed to the limitations the conforming basis functions have when advecting the elevation field. Because these continuous functions take information from neighbouring elements isotropically, their performance may be described as centered.

Ideally such advection of the elevation field would be dealt with purely in an upwind fashion (introducing some diffusion), for instance by using the same non-conforming basis functions as used for the velocity field, but then this combination of basis functions would not have the same desirable behaviour of the conforming/non-conforming combination being investigated here.

Thus, as can be clearly seen in the figure, wave energy is lost into a considerable wake that may be seen to follow the cosine disturbance as it propagates along the equator, and can be compared with the similar ‘erosion’ found in [27] when tackling the same problem.

However, very little energy is lost from the computational region as a whole through the effects of dissipation. At the point at which the snapshot of the solution shown in Figure 6 was taken, less than 0.05% of the original energy had been lost. Mass fluctuations throughout the solution duration were completely negligible.

### Test Case Five: Zonal Flow over an Isolated Mountain

This test case again consists of a solid body rotation or zonal flow

$$\begin{aligned} u &= u_0 (\cos \theta \cos \alpha + \sin \theta \cos \lambda \sin \alpha) \\ v &= -u_0 \sin \lambda \sin \alpha \end{aligned} \quad (8.5)$$

with the corresponding geostrophic height field given by

$$gh = gh_0 - \left( a \Omega u_0 + \frac{u_0^2}{2} \right) (-\cos \lambda \cos \theta \sin \alpha + \sin \theta \cos \alpha)^2 \quad (8.6)$$

where  $\alpha = 0$ ,  $h_0 = 5960 \text{ m}$  and  $u_0 = 20 \text{ m s}^{-1}$ .

The surface, or mountain height, is given by

$$H_s = H_0 \left( 1 - \frac{r}{R} \right) \quad (8.7)$$

where  $H_0 = 2000 \text{ m}$ ,  $R = \pi/9$  and

$$r^2 = \min [ R^2, (\lambda - \lambda_c)^2 + (\theta - \theta_c)^2 ] \quad (8.8)$$

with a disturbance center of  $(\lambda_c, \theta_c) = (0, \pi/6)$ .

The results for this test case, which were achieved with a little diffusion ( $\nu = 1 \times 10^6 \text{ m}^2 \text{ s}^{-1}$ ) to stabilize the solution such that a reasonable duration could be obtained, can be seen in Figures 7 and 8 for the geopotential height and velocity norm fields respectively. The latter being just a contour field generated from the Euclidian magnitude of the velocity vectors located at the mid-points of the element's sides -plotting the velocity vectors themselves would have been impractical.

In Figure 7 the disturbance to the originally uniform geostrophically balanced flow (where all contours are horizontal) caused by the presence of the mountain is clearly visible. Note also the propagation of the disturbances below the equator -the mountain itself being located in the northern hemisphere. These results are very comparable to those obtained by other investigators using other methods, for example with finite volumes [3], [27], and finite elements [17]. Note also the very high wind speeds that occur in the lee of the mountain, as Figure 8 clearly indicates.

### Test Case Six: Rossby Haurwitz Wave

Rossby-Haurwitz waves are analytic solutions of the non-linear barotropic vorticity equation on the sphere [...] they are not analytic solutions of the shallow water equations [...] but have become *de facto* standard test cases [for shallow water models on the sphere] [29]

The initial velocity field is non-divergent

$$\begin{aligned} u &= a \omega \cos \theta + a K \cos^{R-1} \theta (R \sin^2 \theta - \cos^2 \theta) \cos(R\lambda) \\ v &= -a K R \cos^{R-1} \theta \sin \theta \sin(R\lambda) \end{aligned} \quad (8.9)$$

with a height field given by

$$gh = gh_0 + a^2 A(\theta) + a^2 B(\theta) \cos(R\lambda) + a^2 C(\theta) \cos(2R\lambda) \quad (8.10)$$

where

$$\begin{aligned} A(\theta) &= \frac{\omega}{2} (2\Omega + \omega) \cos^2 \theta \\ &\quad + \frac{1}{4} K^2 \cos^{2R} \theta [(R+1) \cos^2 \theta + (2R^2 - R - 2) - 2R^2 \cos^{-2} \theta] \\ B(\theta) &= \frac{2(\Omega + \omega) K}{(R+1)(R+2)} \cos^R \theta [(R^2 + 2R + 2) - (R+1)^2 \cos^2 \theta] \\ C(\theta) &= \frac{1}{4} K^2 \cos^{2R} \theta [(R+1) \cos^2 \theta - (R+2)] \end{aligned} \quad (8.11)$$

where  $\omega = K = 7.848 \times 10^{-6} \text{ s}^{-1}$  and  $h_0 = 8 \times 10^3 \text{ m}$  with a wave number of  $R = 4$  chosen for the initial condition.

In Figures 9 and 10 can be seen the very periodic structure of the Rossby-Haurwitz wave in both the geopotential height and the velocity norm fields. The choice of wavenumber  $R = 4$  has clearly resulted in each pattern occupying  $2\pi/4 = \pi/2$  of longitude.

Even with the comparatively coarse mesh used for this test case the results obtained compare well with those from other methods/investigators [17, 27, 3].

Note that as with the previous test case, the same small amount of diffusion was needed to stabilize the solution to obtain a reasonable duration. It should be mentioned that the solution did eventually 'blow-up' shortly after the results shown were taken.

## Test Case Seven: 500 mbar Geopotential Height and Wind Field Initial Conditions

The values chosen for this test case were taken from the ECMWF data archive, the following extract from the header of one of the ECMWF files used

Value 1 of level (Code Table 3).	500
Value 2 of level (Code Table 3).	0
Year of reference time of data.	1 (2001)
Month of reference time of data.	11
Day of reference time of data.	1
Hour of reference time of data.	0
Minute of reference time of data.	0
Time unit (Code Table 4).	1

indicates the exact time for which the 500 mbar initial data used correspond, namely midnight before the first day of November 2001.

Figures 11 and 12 show contour plots of the geopotential height evolved from the 500mbar initial data at roughly daily intervals for the following 5 days, with a diffusion of  $2 \times 10^6 \text{ m}^2\text{s}^{-1}$  used to stabilize the results.

Owing to the relative coarseness of the mesh used it is difficult to pick out anything but the most large-scale trends in the synoptic behaviour, though a developing wave may be seen to start propagating westwards in the elevation data around the south pole.

It should be noted that data could only be extracted from the encoded ECMWF files in the form of values on a ‘lat-long’ (latitude-longitude) grid. Thus it was necessary to interpolate such data onto the equivalent lat-long positions of the mesh nodes actually used in the computations.

Because of the severe distortion regions around the poles undergo when the sphere is projected onto a plane, slight zonal variations in position near the poles correspond to huge variations in longitude, this meant that the interpolated values used to initialize the velocity and elevation fields in the immediate vicinity of the poles were prone to serious error.

In the experiments with test case 7, it was generally found that the instabilities initiated by such errors tended to bring about the destruction of the solution. The location of these errors was especially unfortunate, because given that integrations over finite elements adjoining the poles tend to be more ‘extreme’ anyway, owing to the presence of functions that are singular at such poles in the integrands, the solution is especially sensitive here.

Furthermore, the prospects for using viscous diffusion to smooth out the often violent behaviour of the solution caused by the initial data interpolation errors is limited by the fact that the diffusive term itself is poorly behaved around the poles because of the integrand’s dependence on the reciprocal cosine of the latitude, see equation (7.24).

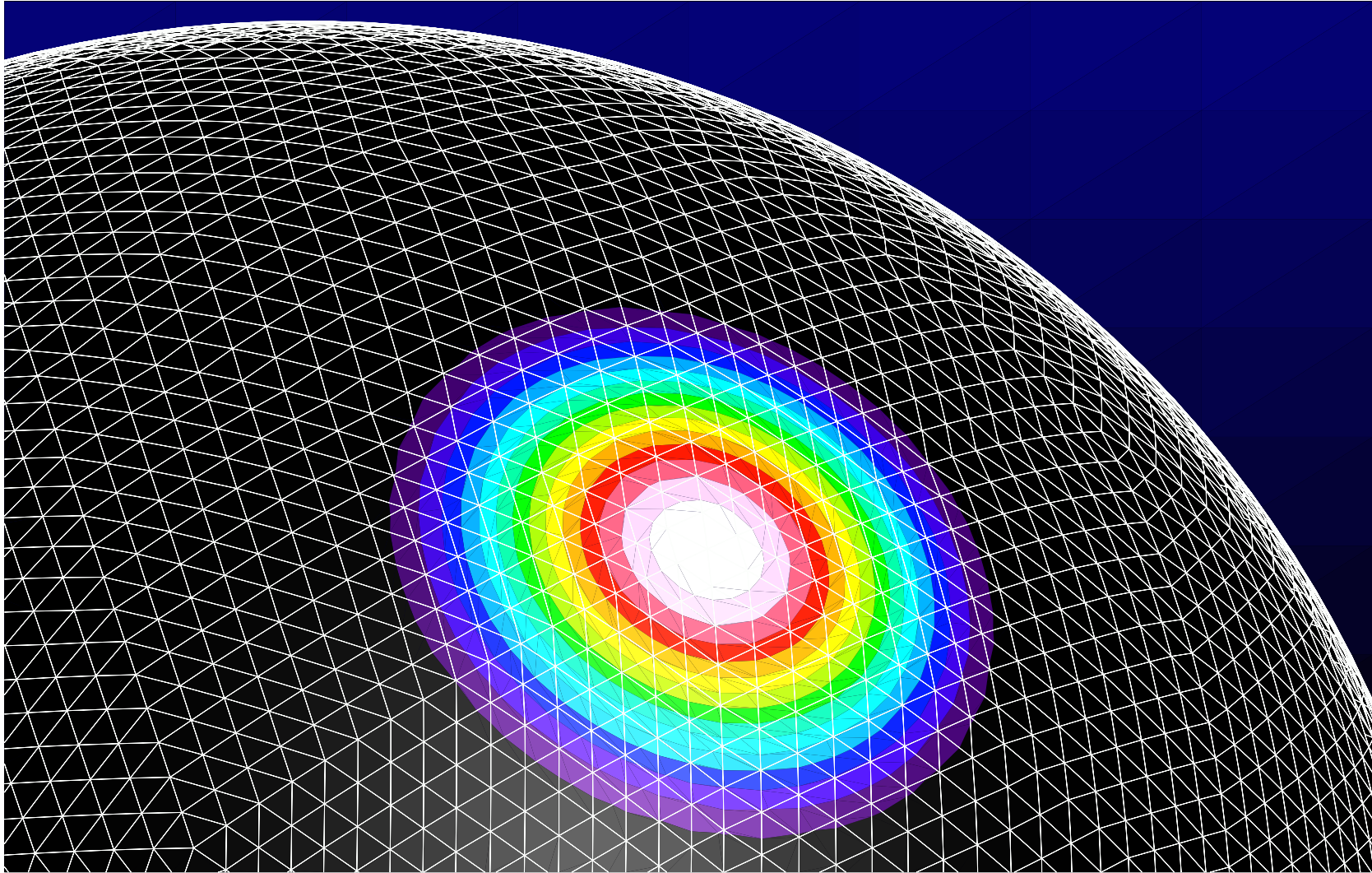


Figure 5: Illustration of the structured 20480 element mesh. (Depicting the Initial Conditions for the Geopotential Height of Williamson Test Case 1: Pure Advection of a Cosine Bell)

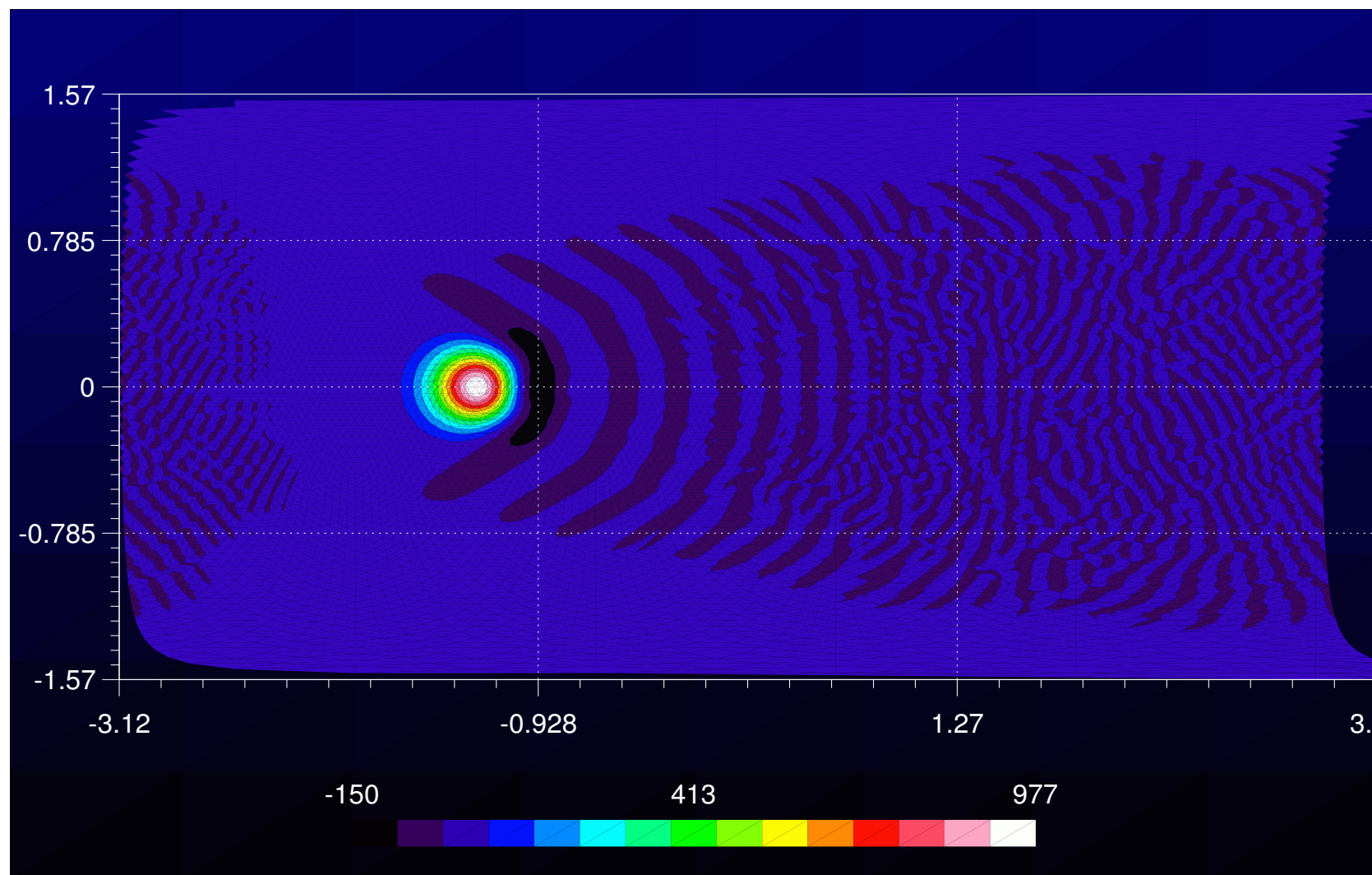


Figure 6: Geopotential Height [ $m^2/s^2$ ] for Williamson Test Case 1: Pure Advection of a Cosine Bell on a structured 20480 element mesh after  $3000 \times 200 \text{ sec} \approx 7 \text{ days}$  plotted on a Latitude-Longitude (vertical-horizontal) Grid

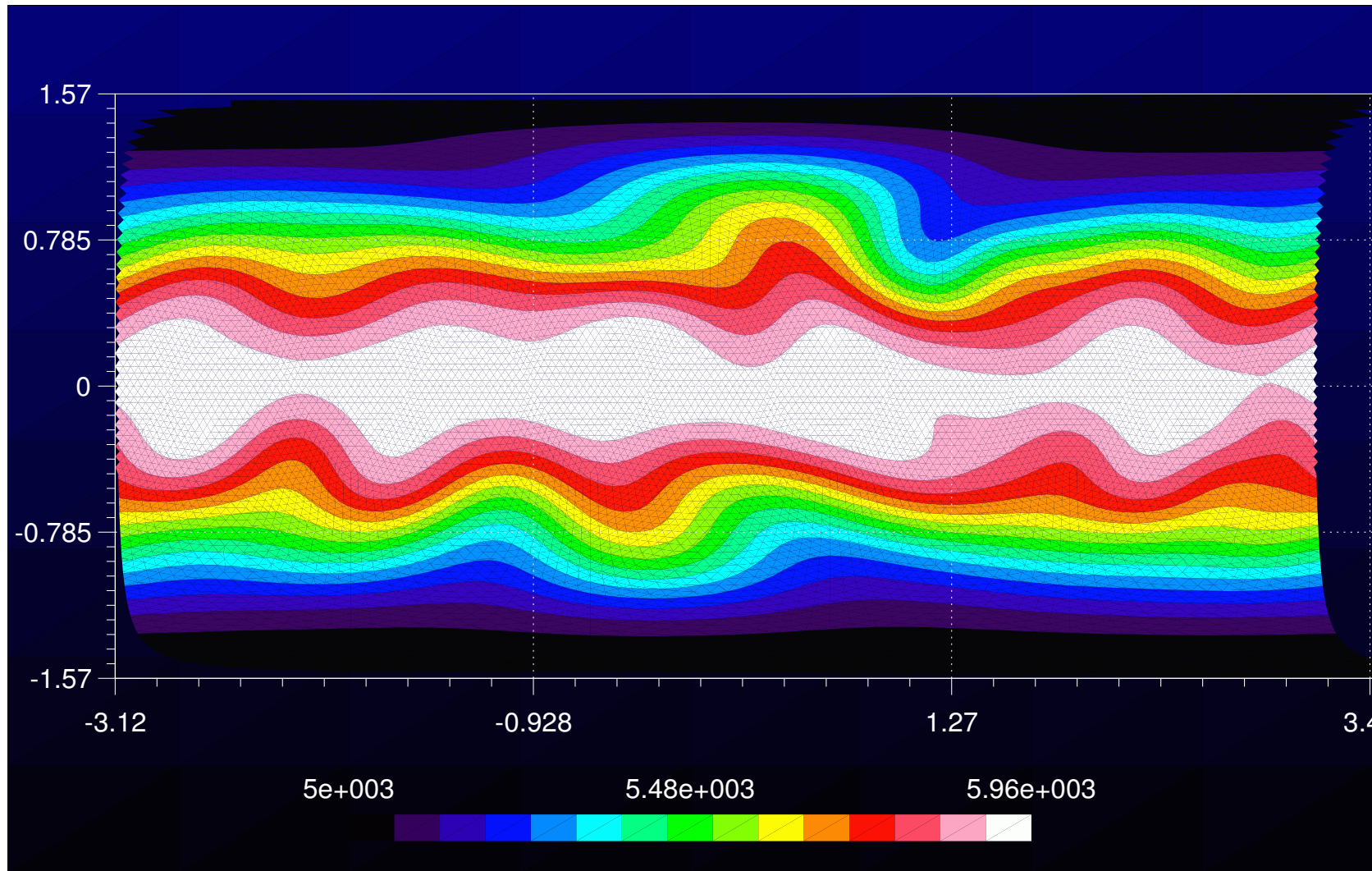


Figure 7: Geopotential Height [ $m^2/s^2$ ] for Williamson Test Case 5: Flow over a Gaussian Hill on a structured 20480 element mesh after  $4000 \times 200 \text{ sec} \approx 9.25 \text{ days}$  plotted on a Latitude-Longitude (vertical-horizontal) Grid

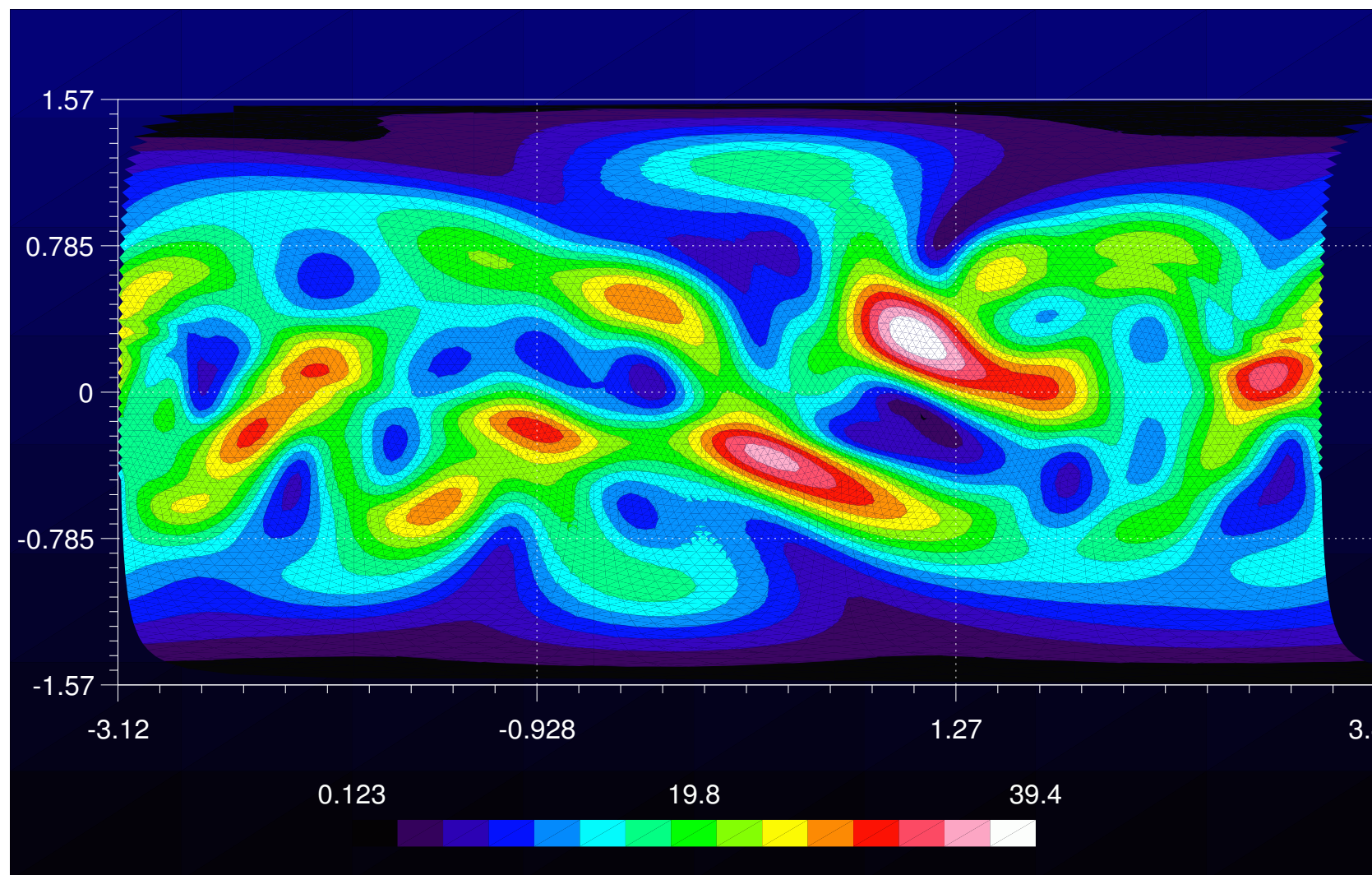


Figure 8: Norm of Velocity [ $m/s$ ] for Williamson Test Case 5: Flow over a Gaussian Hill on a structured 20480 element mesh after  $4000 \times 200 \text{ sec} \approx 9.25 \text{ days}$  plotted on a Latitude-Longitude (vertical-horizontal) Grid

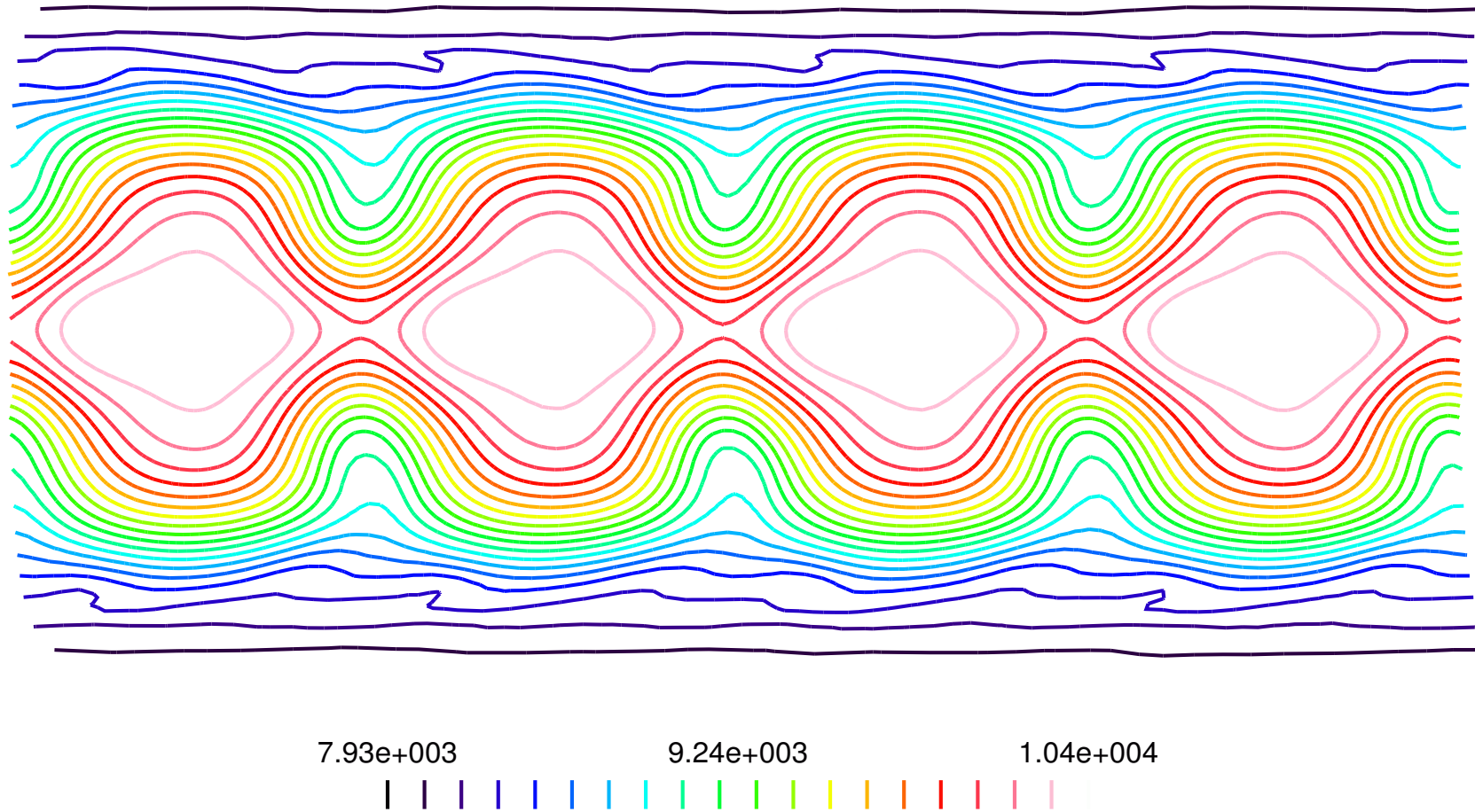


Figure 9: Geopotential Height [ $m^2/s^2$ ] for Williamson Test Case 6: Rossby-Haurwitz Wave on a structured 8192 element mesh after  $2900 \times 400 \text{ sec} \approx 13.5 \text{ days}$  plotted on a Latitude-Longitude (vertical-horizontal) Grid

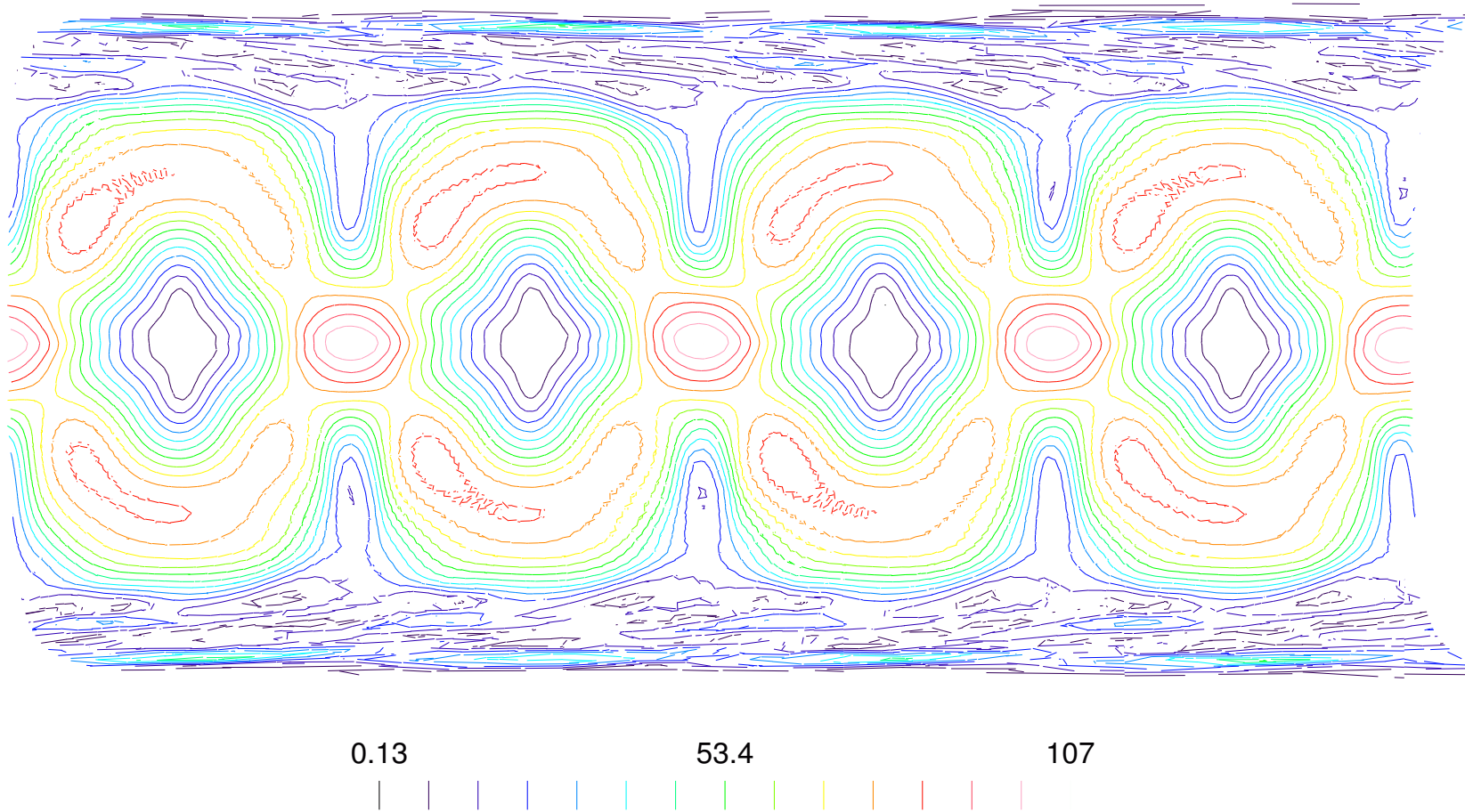


Figure 10: Norm of Velocity [ $m/s$ ] for Williamson Test Case 6: Rossby-Haurwitz Wave on a structured 8192 element mesh after  $2900 \times 400 \text{ sec} \approx 13.5 \text{ days}$  plotted on a Latitude-Longitude (vertical-horizontal) Grid

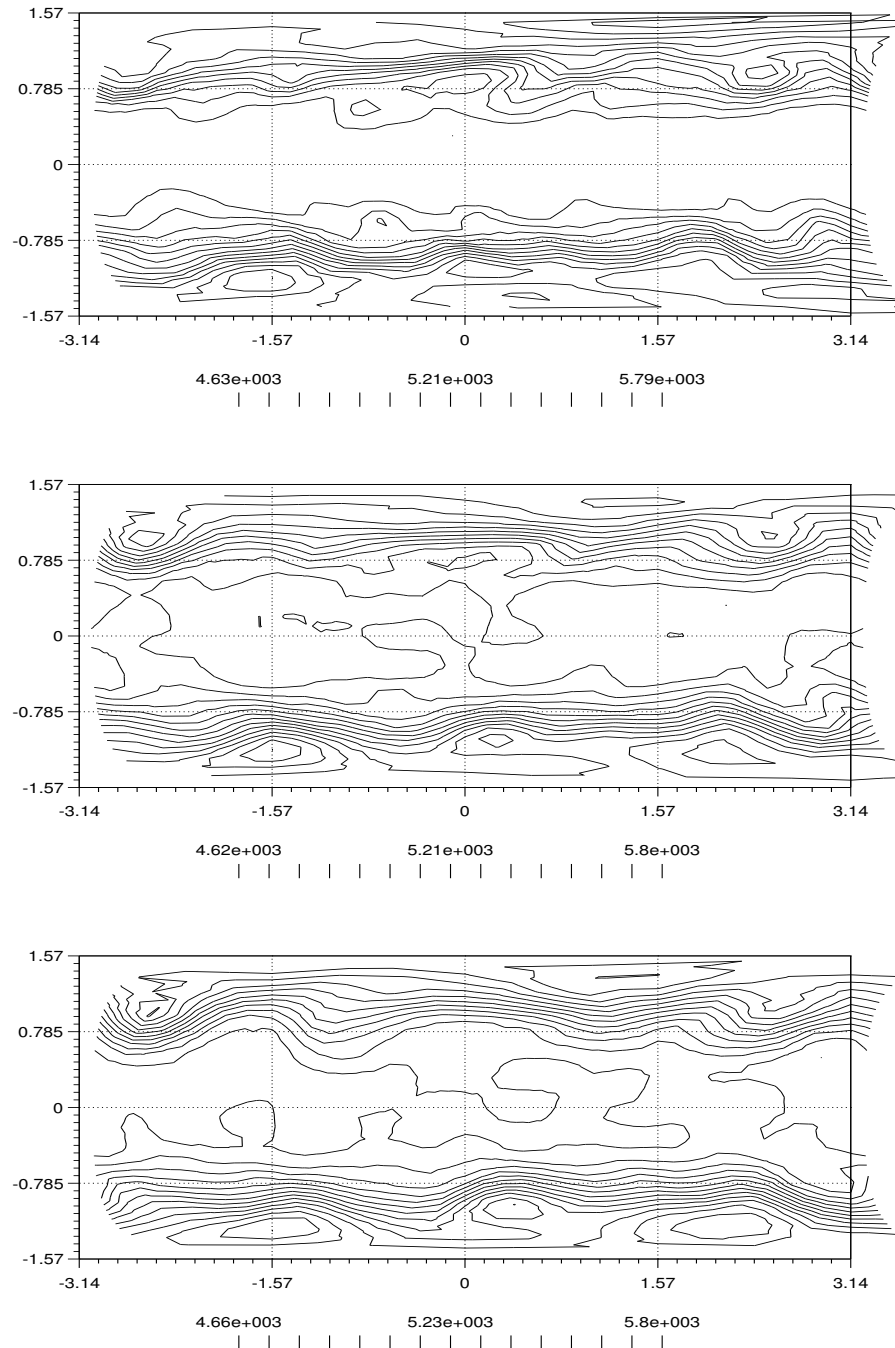


Figure 11: Geopotential Height [ $m^2/s^2$ ] for Williamson Test Case 7: 500mb Data on a structured 8192 element mesh after 0(*top*), 1800, 3600(*bottom*)  $\times 50 \text{ sec} \approx 0, 1, 2 \text{ days}$  plotted on a Latitude-Longitude (vertical-horizontal) Grid

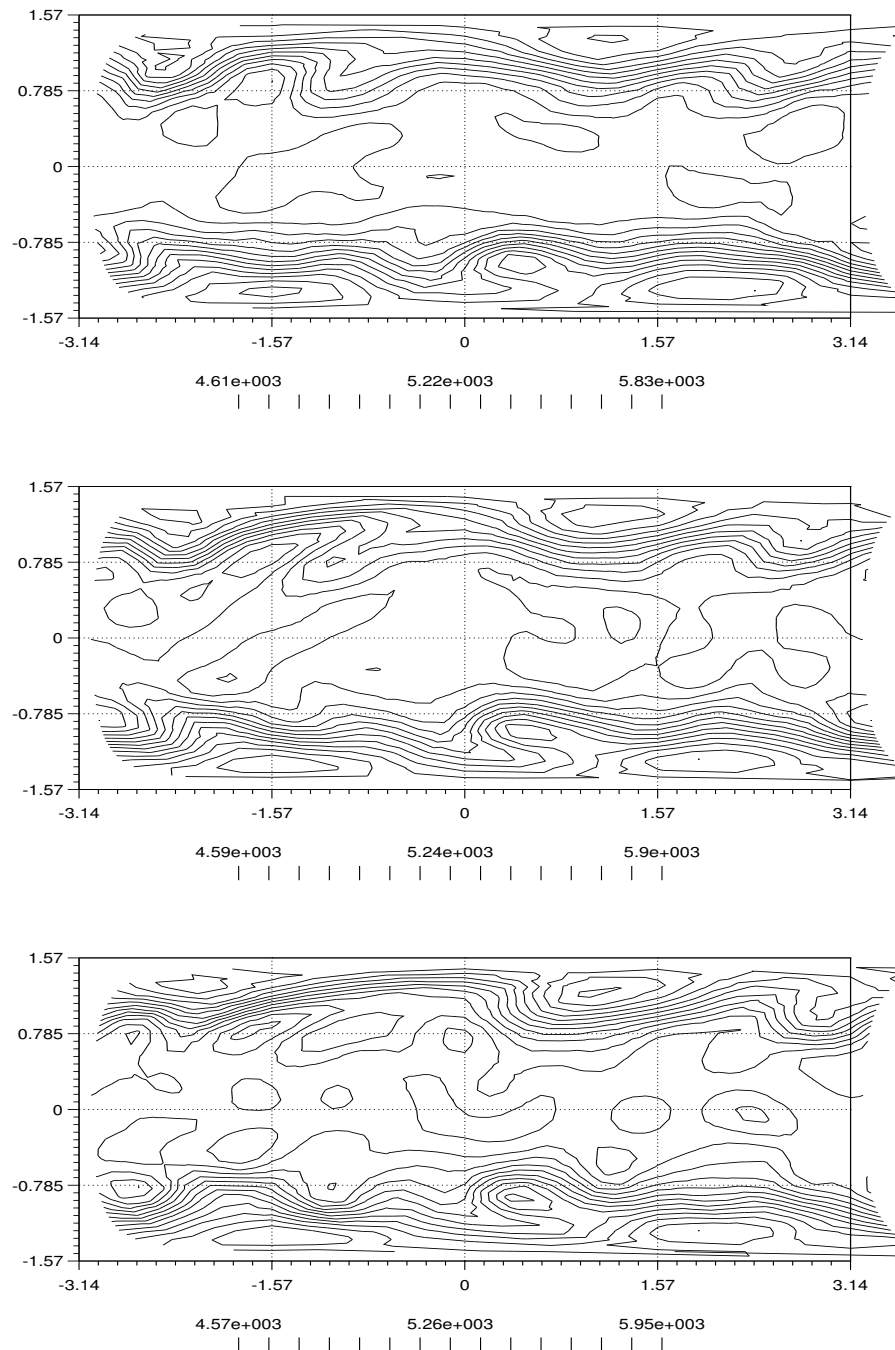


Figure 12: Geopotential Height [ $m^2/s^2$ ] for Williamson Test Case 7: 500mb Data on a structured 8192 element mesh after 5400(top), 7200, 9000(bottom)  $\times 50 \text{ sec} \approx 3, 4, 5 \text{ days}$  plotted on a Latitude-Longitude (vertical-horizontal) Grid

## Conclusions

A novel discontinuous non-conforming/continuous conforming mixed finite element scheme has been introduced to model the synoptic scale motions of a barotropic atmosphere with the velocity and elevation fields of the shallow water equations respectively.

The orthogonality of the non-conforming basis functions, discontinuous except at mid-segments, used in the discretization of the velocity fields enables the construction of a diagonal velocity mass matrix. For the non-orthogonal conforming basis functions, a similar diagonal form was achieved for the elevation mass matrix through the use of mass lumping.

With such diagonal forms, an accurate, relatively cheap Eulerian scheme was presented, with the non-linear terms implemented in a discontinuous Galerkin fashion, that uses a fully explicit third order Adams-Bashforth time integration scheme, with no requirements for matrix inversion, to solve the discrete equations without using a linear solver.

Results were presented for test cases 1, 5, 6 and 7 taken from [29], the latter being liberally interpreted as initializing using genuine 500 mbar geopotential and velocity data for the whole globe.

The results for test cases 1, 5, and 6 were found to be consistent with those found by other workers using other methods applied to the same set of test problems. Results for test case 7 were found to be hindered by problems interpolating lat-long data for the initialization of the elevation and velocity fields.

## Future Work

One of the major frustrations in computing the results presented in this report were the instabilities that often caused the break-up of the solution and necessitated the need to sometimes choose excessively small timesteps or large diffusivities in an attempt to ensure the stability of the solution for the durations required to get reasonable results.

It was often observed that such unstable oscillations occurred in the immediate vicinities of one or other of the poles. This feature can be attributed to problems with the accuracy and stability of the integrations of integrands that are singular at the poles. Thus the computations relied principally on having the poles coincident with nodes of the mesh, such that no Gaussian integration point would actually be placed too close to the polar integrand singularities.

With smaller element sizes however, such Gaussian integration points will inevitably get ever closer to these singularities. Thus a better treatment of such polar integrals is needed. It is suggested that an analytical form could be devised for the integrals over elements with vertices at the poles themselves. The integrations over such elements could then be performed in the computations merely by substitution of the respective element's geometric parameters into the derived analytic

formula, with no need to simply 'hope' that things won't blow up.

Of course, with respect to the results of test case 7, improved results could more immediately be obtained if the problems simply with the interpolations to get the initial data could be overcome, or circumvented. It would also be interesting if a whole sequence of, perhaps daily, real weather data could be extracted from archives with which to compute the  $L_2$  errors of the global elevation and velocity fields as the solution time progresses from that corresponding to the initial data.

Finally, although the use of non-conforming basis functions for velocity fields and full upwinding of the momentum equation is known to dissipate high order oscillations within a solution, it was still found necessary to introduce a general diffusion term to smooth some of the solutions and act against the creation of local velocity extrema. The use and application of this artificial diffusion, however, could also be improved.

The principal attraction of introducing viscosity to an otherwise inviscid problem is to 'smear' out steep velocity (or elevation) gradients which could otherwise give rise to short wavelength instabilities that can initiate the destruction of the solution. However, at present, the code associated with this work applies diffusion in a uniform manner, so smearing is performed globally on the whole solution regardless of whether or not there happens to be a steep solution gradient at a particular location.

Given that the presence of diffusion tends to decrease the overall energy contained within a solution, violating any energy conservation principle, it has been suggested [24], that a more sophisticated application of diffusion, only increasing the viscosity in regions of high shear, could achieve the same results in terms of increased stability through the diffusion of high-order modes, but with a lot less energy loss.

Implementing such a scheme could be relatively easy, with simply the need to establish some form of linear, or otherwise, dependence of the viscosity to be applied at a given location to the elevation or velocity gradients (or a combination of both) there.

## References

- [1] A. Arakawa. Computational design for long-term numerical integration of the equations of fluid motion: Two-dimensional incompressible flow. Part I. *Journal of Computational Physics*, 1:119–143, 1966.
- [2] M. Baines. *Moving Finite Elements*. Oxford Uni. Press, 1994.
- [3] L. Bonaventura, L. Kornbluh, T. Heinze, and P. Ripodas. A semi-implicit method conserving mass and potential vorticity for the shallow water equations on the sphere. *Int. J. Numer. Meth. Fluids*, 47:863–869, 2005.
- [4] J. Cote, M. Roch, A. Staniforth, and L. Fillion. A variable-resolution semi-lagrangian finite-element global model of the shallow-water equations. *Mon. Weath. Rev.*, 121:231–243, 1993.
- [5] M.J.P. Cullen. Integrations of the primitive equations on a sphere using the finite element method. *Quart. J. Roy. Meteorol. Soc.*, 100:555–562, 1974.
- [6] M.J.P. Cullen. On the use of artificial smoothing in galerkin and finite difference solutions of the primitive equations. *Quart. J. Roy. Meteorol. Soc.*, 102:77–93, 1976.
- [7] M.J.P. Cullen. Forecasting and general circulation results from finite element models. *Quart. J. Roy. Meteorol. Soc.*, 105:571–592, 1979.
- [8] B. Cushman-Roisin. *Introduction to geophysical fluid dynamics*. -. Prentice-Hall, 1994.
- [9] D.R. Durran. The third-order adams-bashforth method: An attractive alternative to leapfrog time differencing. *Mon. Weath. Rev.*, 119:702–720, 1991.
- [10] D.R. Durran. *Numerical methods for wave equations in geophysical fluid dynamics*. Springer Press, 1999.
- [11] A. Fournier, M.A. Taylor, and J.A. Tribbia. The spectral element atmosphere model (seam): High-resolution parallel computation and localized resolution of regional dynamics. *Mon. Weath. Rev.*, 132:726–748, 2004.
- [12] E. Hanert. *Towards a Finite Element Ocean Circulation Model*. PhD thesis, Université catholique de Louvain, Belgium, 2004.
- [13] E. Hanert and V. Legat. How to save a bad element with weak boundary conditions. *Computers and Fluids*, 35:477–484, 2006.
- [14] E. Hanert, D.Y. LeRoux, V. Legat, and E. Deleersnijder. Advection schemes for unstructured grid ocean modelling. *Ocean Modelling*, 7:39–58, 2004.

- [15] J.R. Holton. *An introduction to dynamic meteorology*. -. Academic Press, 1979.
- [16] Y. Kurihara. Numerical integration of the primitive equations on a spherical grid. *Mon. Weath. Rev.*, 93:399–415, 1965.
- [17] M. Lauter and D. Handorf. A parallel adaptive barotropic model of the atmosphere. *J. Comp. Phys.*, 223:609–628, 2007.
- [18] M. Lauter and D. Handorf. A parallel adaptive barotropic model of the atmosphere. *J. Comp. Phys.*, 223:609–628, 2007.
- [19] D. LeRoux, E. Hanert, V. Rostand, and B. Pouliot. Impact of mass lumping on gravity and rossby waves in 2d finite-element shallow-water models. *International Journal for Numerical Methods in Fluids*, Submitted:–, 2008.
- [20] M.N. Levy, D.N. Ramachandran, and H.M. Tufo. High-order galerkin methods for scalable global atmospheric models. *Computers and Geosciences*, 33:1022–1035, 2007.
- [21] S.J. Lin and R.B. Rood. An explicit flux-form semi-lagrangian shallow-water model on the sphere. *Quart. J. Roy. Meteorol. Soc.*, 123:2477–2498, 1997.
- [22] F. Mesinger and A. Arakawa. *Numerical Methods used in Atmospheric Models*. GARP Publications Series No. 17. WMO - ICSU, 1976.
- [23] J. Pedlosky. *Geophysical Fluid Dynamics*. Springer Press, 1987.
- [24] J. Smagorinsky. General circulation experiments with the primitive equations. *Mon. Weath. Rev.*, 91:99–164, 1963.
- [25] A.N. Staniforth and H.L. Mitchell. A semi-implicit finite-element barotropic model. *Mon. Weath. Rev.*, 105:154–168, 1977.
- [26] M. Taylor, J. Tribbia, and M. Iskandarani. The spectral element method for the shallow water equations on a sphere. *J. Comp. Phys.*, 130:92–108, 1997.
- [27] J. Thuburn. A pv-based shallow-water model on a hexagonal-icosahedral grid. *Mon. Weath. rev.*, 125:2328–2347, 1997.
- [28] J.J. Westerink, R.A. Luetich, J.K. Wu, and R.L. Kolar. The influence of normal flow boundary conditions on spurious modes in finite element solutions to the shallow water equations. *Int. J. Numer. Meth. Fluids*, 18:1021–1060, 1994.
- [29] D.L. Williamson, J.B. Drake, J.J. Hack, R. Jakob, and P.N. Swarztrauber. A standard test set for numerical approximations to the shallow water equations in spherical geometry. *Journal of Computational Physics*, 102:211–224, 1992.